PHASE EQUILIBRIA STUDIES IN WATER-METHANE SYSTEM: STRUCTURAL MEMORY-EFFECT OF WATER ON HYDRATE RE-FORMATION

A Thesis

by

BRICE YOONSHIK KIM

Submitted to the Office of Graduate and Professional Studies of
Texas A&M University
in partial fulfillment of the requirements for the degree of

MASTER OF SCIENCE

Chair of Committee,	Ibrahim Yucel Akkutlu
Committee Members,	Maria Antonieta Barrufet
	Marcelo-Javier Sanchez
Head of Department,	Alfred Daniel Hill

December 2014

Major Subject: Petroleum Engineering

ABSTRACT

Naturally-occurring hydrates are promising resources. The potential value of gas accumulation in naturally-occurring gas hydrates can exceed 16 equivalent trillion tons of oil. There are many accurate findings on properties of gas hydrates. This is especially true for laboratory formed gas hydrates, but many of definite physical properties are not completely understood. More importantly, in terms of production point of view, the conditions of formation as well as stable existence of naturally occurring gas hydrate deposits are still not well known. These difficulties are further complicated by the structural memory-effect of water on hydrate re-formation, a phenomenon in which previously hydrate-formed liquid re-forms hydrate more readily. This research mainly focused on the stability of hydrate existence in various condition to determine how the water-gas system with previous hydrate history affects the re-formation of hydrates, both experimentally and numerically using the molecular dynamic simulation.

DEDICATION

This work is dedicated to Tae-Woong Kim, my father and Mi Alisa Mun, my mother. It is my deepest gratitude and sincerest affection that I dedicate this thesis to my parents. My parents deserve the hugest mention for supporting me and standing by me. Lastly, I would like to give sincerest thanks to the almighty God.

ACKNOWLEDGEMENTS

I would like to thank Dr. Akkutlu for giving me this opportunity to learn and get experiences at hydrate lab. This works could not have been done without his valuable supports and insights. I would also like to thank Dr. Makogon for his guidance, and valuable comments towards completing this research as well as enlightening me with backgrounds on hydrates. Without his guidance I could not have finished this research. I would like to thank Dr. Bui for greatly assisting me in creating simulation box for the MD simulation.

I would like to thank my committee members, Dr. Barrufet, and Dr. Marcelo-Sanchez for their guidance and support in completing this thesis.

Thanks also go to my friends and colleagues and the department faculty and staff for making my time at Texas A&M University a great experience

NOMENCLATURE

SO_2	Sulfur Dioxide
CH4	Methane
MD	Molecular Dynamic
DAQ	Data Acquisition
GROMACS	GROningen Machine for Chemical Simulations (Software)
SPC	Simple Point Charge
TIP	Transferable Intermolecular Potential
OPLS/AA	Optimized Potentials for Liquid Simulations / All-Atoms
REV	Representative Elementary Volume

TABLE OF CONTENTS

Page

LIST OF FIGURES

LIST OF TABLES

Page

CHAPTER I

INTRODUCTION

Naturally-occurring hydrates are one of the most promising natural sources for the coming age. It is often described as the burning ice by public media and articles. The potential value of gas accumulation in naturally-occurring gas hydrates can exceed 16 equivalent trillion tons of oil. Near 97% of these reserves are located offshore, mainly in continental shelf-oceanic slope transition zones, only 3% on land. These deposits and formation zone can be estimated if the depth of water, sea bed temperature and thermal gradients are known. (Makogon, Holditch & Lee 2001).

Four conditions must be present in order for gas hydrate to form. 1) There must be hydrate forming gas, free or dissolved, 2) there also must be water 3) water and gas must be under hydrate stable pressure, 4) and the environment must provide sufficient heat transfer. Under these conditions, this solid clathrate compound can entrap significant amounts of gas. However there are still many obstacles in implementing production of energy resource from this promising energy packed clathrate.

There are many accurate findings on properties of gas hydrates. This is especially true for laboratory formed gas hydrates, but many of definite physical properties, such as bonding strength of hydrogen bonds and physical phenomena that entrap guest molecules are not completely understood. More importantly, in terms of production point of view, the conditions of formation as well as stable existence of naturally occurring gas hydrate deposits are still unknown.

Gas hydrates in nature are typically found in one of the following three types of reservoirs; coarse grained, fine grained, and fractured. (Collett *et al*., 2008). The notable coarse grained reservoirs are Mallik permafrost site in Canada and Nankai Trough in offshore Japan. Gas hydrate formation in these sites can be characterized as having pore filling characteristics and occasionally reaches the maximum hydrate saturation of 80% (Dallimore et al., 1999; Winters et al., 1999).

There are several known challenges and uncertainties related to production from gas hydrates. The challenges in studying gas hydrates production begins with uncertainty in energy assessment from naturally occurring gas hydrates around the globe. (Sloan and Koh, 2008), Sampling sediment samples suffers from unavoidable change in effective stress and strains from coring tools to determine correct production conditions (Lunne et al, 2006). Liquid water increase and gas expansion due to dissociation leading to uncertainty in determination of reservoir water ionic concentration as released water from hydrates dilutes reservoir water (Moridis et al, 2010). Most importantly, the gas hydrates are well known for hindering production of natural gas due to re-formed hydrates obstructing the flow of natural gas through the production pipe. (Makogon, 1997)

CHAPTER II

LITERATURE REVIEW

2.1 History

The first documented laboratory formed gas hydrate takes back as early as 1778 by Joseph Priestley when he obtained bubbling SO_2 at 0℃ through water at atmospheric pressure and low room temperature (Priestley, 1778). About 33 years later in 1811, Humphrey Davy formed crystals of aqueous chlorine and were called hydrates of gas. However, the finding did not attract scientists of the time and was almost forgotten as only 56 papers from 16 authors published in regards of hydrates from 1778 to 1934 (Makogon, 2010).

The more active research of gas hydrates started in 1934, when Hammerschmidt inspected and published a report concerning solid plugs that formed in pipelines during the winter time, which later was determined to be gas hydrates (Hammerschmidt 1934). This urgency led to rapid growth in research interests on gas hydrates. Detailed conditions of the hydrate formation were needed to be determined, thus the early stage of active hydrate research was catalyzed primarily to study formation preventions in the pipelines instead of determining energy productions. From 1934 to 1965, 144 papers were published marking the early active research stage on hydrates (Makogon, 2010).

The more recent and current era of hydrate study began in 1963 when the Markhinskaya well in the north-western part of Yakutia, Siberia revealed a section of rocks at the depth of 1450m with temperature at 0℃. The condition of the rock

formations matched those of hydrate formations. This discovery led to hypothesize the natural existence of the gas hydrate in 1965 (Makogon 1965) with confirming experiments at the Gubkin Institute of Oil and Gas in Moscow in 1966 (Makogon 1966), the scientific discovery of naturally-occurring gas hydrates was recorded in 1969. There have been more than 14,000 papers concerning gas hydrates since 1965.

2.2 Intrinsic Properties and Characteristics

2.2.1 General Properties

Hydrates are solid metastable compounds. There are two components that must coexist in order to form gas hydrate; water and gas. It is also important to note that the gas hydrate stability is dominantly dependent on, pressure and temperature. The condition of hydrate formation and its stability zone are shown in Figure 1. It can be seen that methane hydrates can form under high pressure and it is even possible to form methane hydrates at a room temperature as long as the pressure is sufficient enough. It is also possible for ice and methane hydrate to coexist in a system.

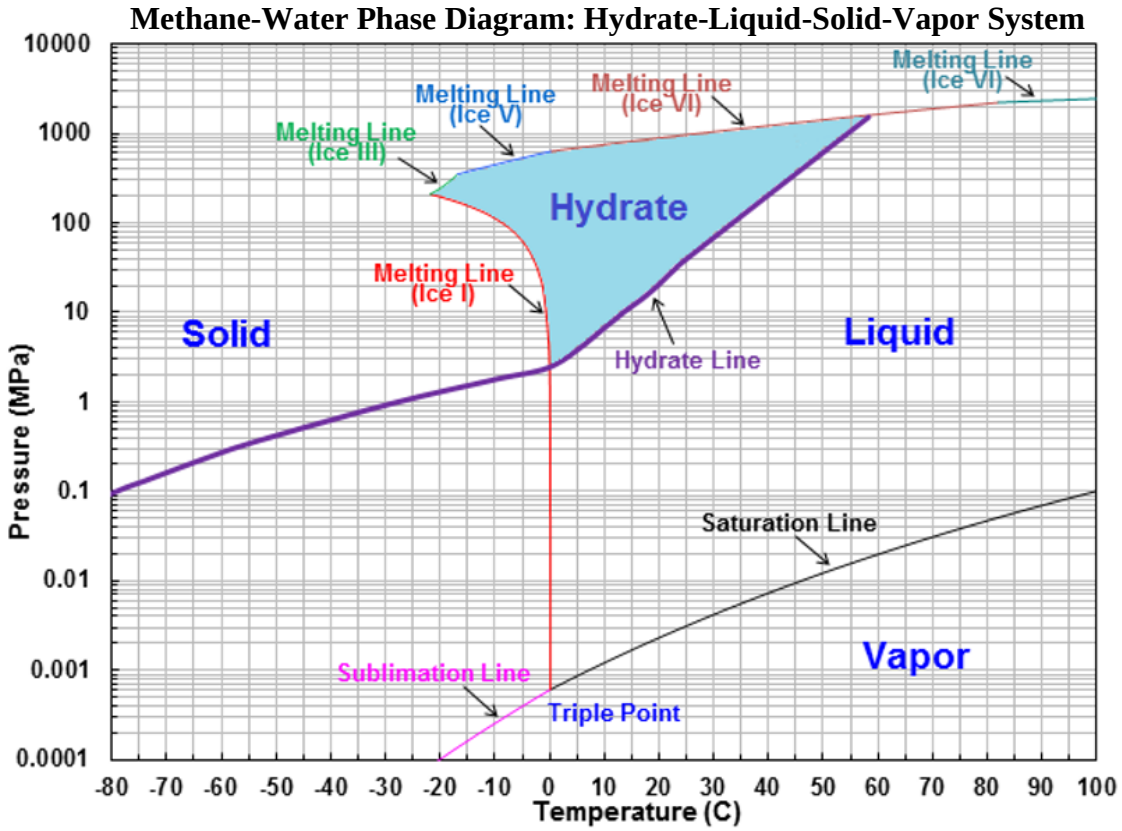

Figure 1: Conditions for methane hydrate formation in pure methane and water system.

Gas hydrate is the compound of molecular type and is formed due to the Van der Waals attraction between molecules, with hydrogen bonded water molecules building cage networks to entrap gas molecules as shown in Figure 2. Covalent bonds are absent in the gas hydrates (Makogon, 2010). There are three known structures of hydrates, Structure I, II and H. These structures were determined by the works of Von Stackelberg group (1973-1994) and Davidson and Ripmeester group (1973-1994). Hydrate structure, shape and size are determined by the energy of the enclathrated hydrate forming guest molecules. Most commonly occurring structures of hydrates are of Structure I and II. The size and shapes of hydrates are shown in Figure 2 below

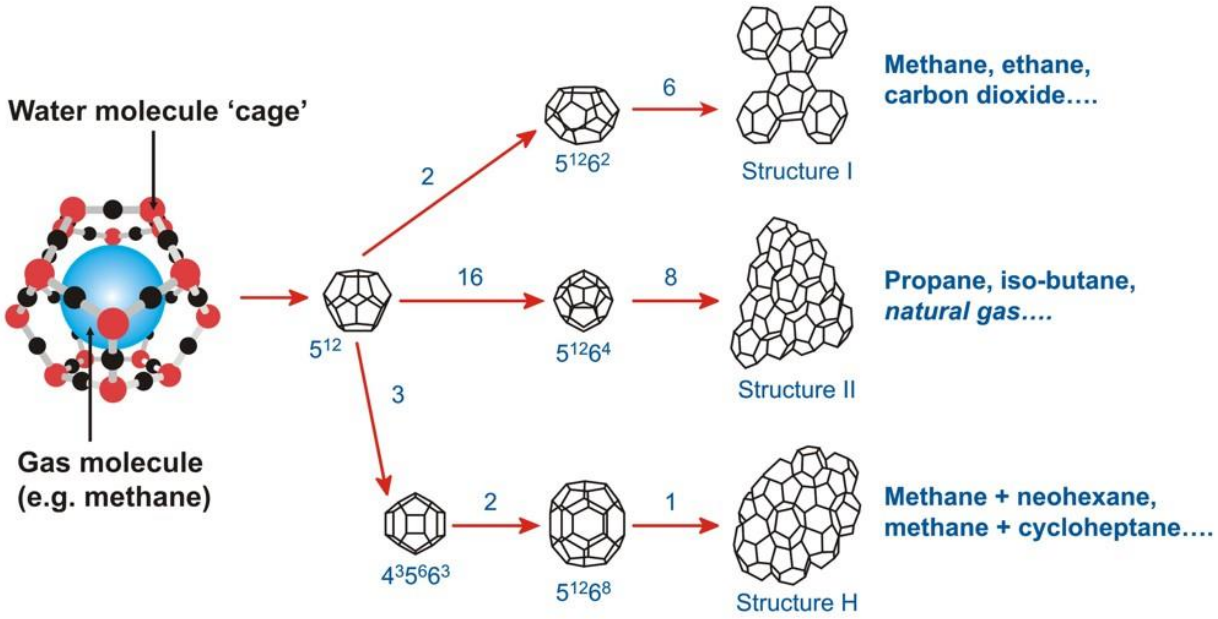

Figure 2: Different types of hydrate structures with different types of guest molecules that it can host.
(http://www.pet.hw.ac.uk/research/hydrate/images/hydrates/structures_large.jpg)

The sizes of the dodecahedral cavities formed by water molecules in hydrates are sufficient to accommodate various molecules. They are notably argon (0.308 nm), krypton (0.338 nm), xenon (0.38 nm), methane (0.406 nm) and hydrogen sulfide (0.42 nm) (Makogon 1997). Overall, gas hydrates are capable of accommodating gas volatile liquids no larger than 0.83nm (Makogon et al 2001).

In general, one unit volume of methane hydrate contains 164.6 unit volumes of methane gas at standard conditions. In solid hydrate state, water occupies 80% of the volume, and the rest, 20%, is occupied by methane. The volume of methane hydrate increases by 26-32% when hydrate forms, compared to approximately 9% increase from water to ice (Makogon et al 2001). Gas hydrate formation is an exothermic process, and the dissociation is an endothermic process. Due to these characteristics, gas hydrate

reformation may occur as it dissociates in closed surrounding, such as in gas pipelines or in pore network. This is due to the fact that the endothermic process of dissociation may decrease temperature of the nearby surroundings which then create ideal condition, i.e. low temperature, for gas hydrate or ice formation (Seol and Myshakin 2011). Once the gas hydrate is formed, about 6-10% of the energy contained within the gas hydrate is required to decompose in natural condition. Dissociation in a closed volume generates pressure ranging from 2.6MPa up to 140MPa (Makogon et al 2001).

2.2.2 Hydrogen Bond and Water

Water is considered to be the single most important former of any gas hydrates. Water molecules are formed due to a special case of intermolecular bonds known as the hydrogen bond. When hydrogen is attached directly to one of the most electronegative elements, (such as Oxygen, Nitrogen, and Fluorine) the difference in partial charges lead to attraction of the atoms. It is noted that the energy required to break the hydrogen bond is 5 Kcal/mole. The hydrogen bond is stronger than Van der Waals bond, 0.3 Kcal/mole, but significantly weaker than covalent bond, 102 Kcal/mole, (Sloan and Koh, 2008).

This molecular attraction is known as the hydrogen bond leads to formation of liquid and solid water. There are about 15 known structures of solid water (Salzmann et al, 2009) also the water molecules are similarly bonded in hydrate by hydrogen bond. (Sloand and Koh, 2008) The ubiquitous hexagonal shaped structure *ih* ice, or ice 1, is shown in Figure 3.

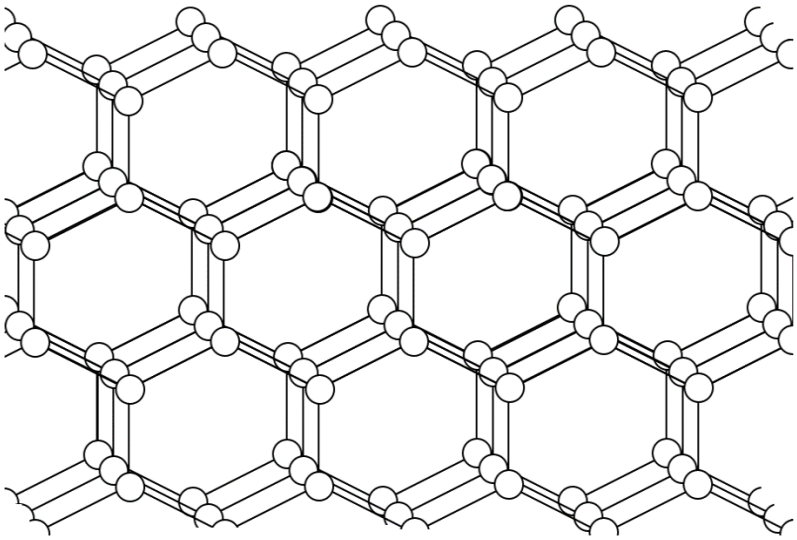

Figure 3: Structure of hexagonal shaped *ih* ice or ice 1

When hydrates form or dissociate, often only hydrogen bond is considered. No chemical bonds need to be broken between hydrogen and oxygen. Van der Waals forces are present but it is often neglected due to its significantly lower bond strength.

In a molecular level, the gas hydrate formation starts with a phenomenon known as hydrophobic hydration. (Frank and Evans, 1945) This is when hydrophobic molecules, such as methane, are trapped inside cages of hydrogen bonded water. It has also been said that the hydrophobic hydration makes the cage network stronger by supporting the case. Without the support of hydrophobic gas, the lattice could collapse into conventional solid water structure. (Sloan and Koh, 2008)

2.2.3 Hydrate Formation and Solubility

Hydrate formation is initiated when there are enough hydrate forming gas molecules in the aqueous solution, thus understanding of gas solubility is important for the understanding hydrate formation.

Solubility values at different conditions can be collected either by experimental approach or by theoretical modeling approach. There are different factors that affect gas solubility in water. The effects of temperature and pressure will be discussed here. The solubility of gas is primarily temperature dependent. Increasing temperature also increases kinetic energy of the gas molecules. This allows gas molecules break free from the intermolecular bonds in the liquid water which enables molecules to enter the vapor phase. Same is true for gas molecules in hydrate state. Hence, gas hydrates become less stable as temperature increases.

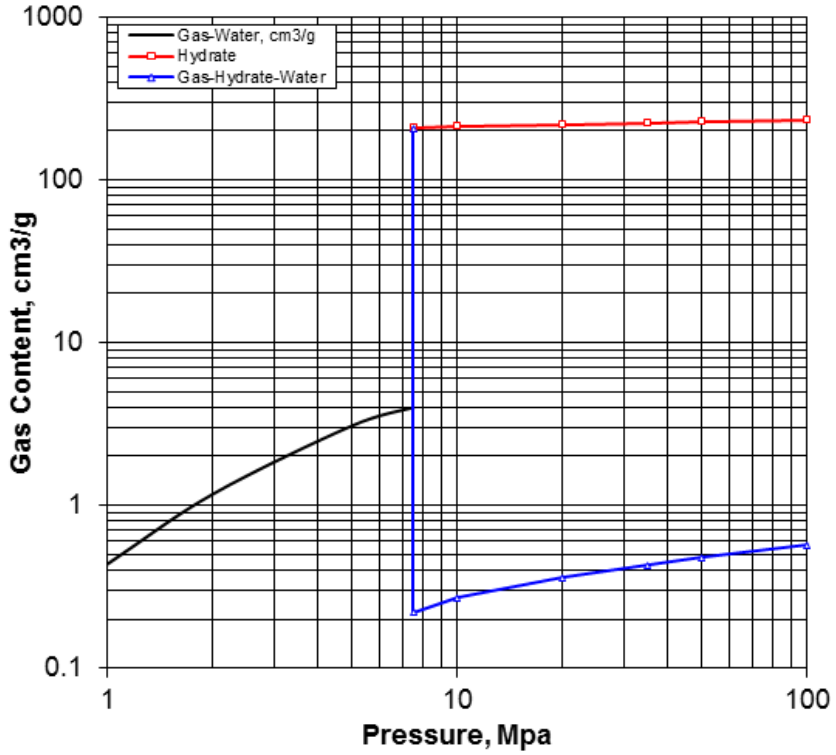

Figure 4: Gas solubility change as gas hydrates form with increasing pressure. (Makogon et al 2001)

In terms of pressure, the solubility of gas in aqueous solution increases as pressure increases. An interesting phenomenon occurs as gas hydrates are starting to form. It has been shown experimentally that as gas hydrate forms, the solubility of gas in water decreases noticeably as shown in Figure 4.

On the contrary the solubility of gas in hydrate increases significantly. This is an indication and confirmation of characteristic of gas hydrate that it can form and be stable while in contact with saturated gas (Makogon 2001). Also, this is the evidence that gas prefers to exist in hydrate state, rather than in the dissolved state. (Makogon 2001 and Servio & Englezos 2002)

2.2.4 Naturally Occurring Gas Hydrate Formation and Habits

Gas hydrates generally exhibit three different traits of behaviors as they form in the sediment. First is that as gas hydrate form, it nucleates on sediment grain boundaries and grow freely into pore space without contacting nearby particles, exhibiting pore filling habit. This particular behavior contributes change in pore fluid bulk stiffness and fluid conduction properties of sediment (Helgerud et al., 1999). The second behavior of gas hydrate is the opposite of the first behavior; the gas hydrate formation makes contact with nearby particles resulting bridging effect. This behavior contributes to change in mechanical stability, usually makes sediment more stable, by becoming load-bearing framework. (Berge et al., 1999, Yun et al., 2005, 2007). The last known common behavior of gas hydrate formation is cementing effect in the sediment. In this particular behavior, gas hydrate formation encircles grains, contributing to increase of sediment shear and bulk stiffness by bonding adjacent grains together. (Dvorkin et al., 1999)

In nature, formation patterns of gas hydrates are varied as shown in Figure 5. Usually in coarse sands, hydrates exhibit disseminated or pore-filling characteristics. Whereas in fine-grained sediments, it exhibits veined or nodule-type of characteristics. It is believed that the hydrates in sediments within the gas hydrate stable zone are formed by dissolved aqueous phase gas. (Buffett and Zatsepina, 2000).

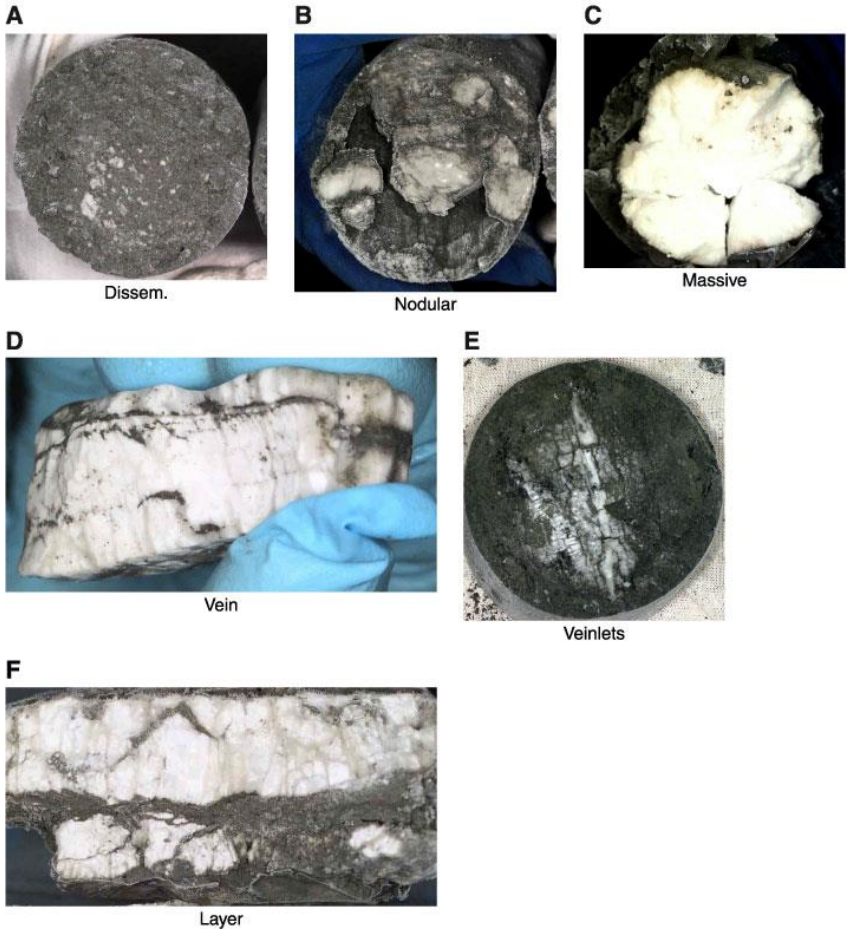

Figure 5: Different formation patterns of gas hydrates in nature. (Tréhu et al, 2003)

From on-site measurements, it can be inferred that when the gas hydrate saturation of the sediment exceeds 25%-30% it can be characterized as load-bearing (Kleinberg and Dai 2005, Lee & Waite 2008), with the exception of high gas flux areas (Bohrmann et al 1998) and where gas is recycled into hydrate stable zone, which then can be characterized as cementing (Guerin et al 1999; Yuan et al 1999).

It has also been suggested that the hydrate sand can be characterized with load-bearing models when the hydrate saturation exceeds 25-30% (Kleinberg and Dai, 2005; Lee and Waite, 2008).

2.2.5 Naturally Occurring Gas Hydrate Production and Challenges

Theoretically, naturally occurring gas hydrates can be produced using three different methods: (1) by depressurization, (2) by thermal stimulation and (3) by injection of inhibitors such as salt (Makogon, 1997). All these methods causes phase shift from a hydrate stable region in the phase diagram causing the dissociation of the hydrate in the sediment. However there are several known challenges and uncertainties related to gas hydrates:

Gas-in-Place Estimates. Even though there are abundant references and estimates by different research groups, there is not a universally established method to calculate gas in place estimates from natural gas hydrates. This also led to uncertainty in how much gas can actually be produced from the naturally occurring gas hydrates (Sloan and Koh, 2008).

Sampling. The sampling of gas hydrate suffers from unavoidable change in effective stress and strains from coring tools (Lunne et al, 2006). This is not a unique challenge that only applies to gas hydrate field sample. It has also been mentioned that natural gas hydrate dissolution leads to increase in liquid water and gas which leads to uncertainty in determination of reservoir water ionic concentration as released water from hydrates dilutes reservoir water (Moridis et al 2010).

Drilling Hazard. The gas hydrate have been recognized as a hazard for drilling and production as it can trigger uncontrollable gas release during drilling. For natural gas hydrate production, the common practice has been to drill through the hydrate bearing sediment with freeze-depressed drilling fluids chilled to below 32^{o}F to prevent

dissociation. This is followed by the well casing using the low heat of hydration cement to prevent hydrate formation. However, the history of natural hydrate production is not long enough to provide a practical production procedures for long-term productions (Moridist et al 2010).

Production Hazards. Production from naturally occurring gas hydrates formed in nodules in the fractures and pore-fillings in the sediment could lead to reservoir subsidence. This subsidence could potentially lead to casing shear and failure, loss of mechanical strength of along the wellbore as the hydrates holding the grains in the reservoir dissociates and weakens the sediment. These issues also lead to development of high pressure along the wellbore (Rutqvist et al., 2008). It has been noted that up to this day, the most effective way to handle reservoir subsidence leading to casing failure is to have strategic well placement and to consider budget for possible well replacement in the event of the failure (Moridis et al., 2010).

2.3 Laboratory Synthesized Gas Hydrates

There are few methods that are used to form hydrates in laboratory environment for study and analysis of behaviors and characteristics. The four well known methods to form gas hydrates in laboratory are; dissolved gas method, partial water saturation method, ice-seeding method and hydrate premixing method.

The methods for forming laboratory gas hydrates that are least of our interests are ice-seeding method and hydrate premixing methods. These methods either uses frozen ice grains or pre-made hydrate grains then mixed with soil and water which then the temperature of the gas pressurized sample contained environment is increased slightly above hydrate stable condition either to provide water from ice to form hydrate or to provide annealing, then the environment is brought down to stable condition to form a representative model of hydrate bearing sediment by forming gas hydrates as small seeds or granular types. These two methods are not in the interest of our group due to its complexity and requirement of low-temperature controlled facility or chamber, which are not available for our group. Furthermore, the formations of naturally occurring hydrate sediments are mostly known to have characteristics of pore-filling, cementing and load-bearing, (Murray et al 2006, Guerin et al 1999, and Helgerud et al 1999) not seeding or granular types. To emulate the formations and characteristics of naturally occurring gas hydrates in the laboratory, the dissolved gas and partial water saturation methods are needed to be considered and detailed discussion are presented in this report.

2.3.1 Dissolved Gas Method

In this method, water is saturated with a hydrate-forming gas by pressurization, and then the gas saturated water is circulated through laboratory packed sediments (i.e. sand pack) under hydrate forming conditions. To accelerate the hydrate formation, CO_2 is often used as it exhibits many similar traits and characteristics of methane but can be dissolved in water at much lower pressure, 2MPa compared to 10MPa of methane. (Buffett, 2000) However, the induction time and detectable hydrate nucleation time can be relatively long when compared with other hydrate forming methods. (Sloan and Koh, 2008). Conceptually, the dissolved gas method is limited to forming hydrate saturation below approximately 60~70%. This method leads to preferential hydrate formation into the pore space. The major advantage of this method is that it closely resembles the natural gas hydrate forming conditions, albeit with requirement of high pressure chamber if methane was to be used for the experiment instead of CO_2 and with much longer nucleation time when compared with partial water saturation method.

2.3.2 Partial Water Saturation Method

In partial water saturation method, sand grains are pre-saturated with water then packed to form partially or fully wet sediment, then pressurized with methane gas and cooled to hydrate stable condition. Depending on the initial water saturation, this method could take just a few days to form hydrate-bearing sediments. (Kneafsey et al. 2007 and Waite et al. 2004). This method leads to preferential hydrate formation between grains, bridging to form load-bearing habit. The major advantage of this method is that it can

mimic naturally occurring hydrate conditions and takes much less time for nucleation to start when compared with dissolved gas method. This was the chosen method for the experiments done in this dissertation.

CHAPTER III

PHASE EQUILIBRIA IN WATER AND GAS CONTACT

3.1 Research Background and Overview

This research mainly focused on understanding phase equilibria of methane hydrates in both free water-gas contact and in pore-space. Many researchers have previously studied the formation and dissociation characteristics of hydrates. However there has not been any research dedicated to the memory effect phenomenon of gas hydrate re-formation. The general consensus among the hydrate researchers suggests that hydrates retain a form of structural memory when they dissociate at moderate temperatures. This phenomenon allows the previously hydrate-formed liquid to form hydrate again but with much less energy than that of the prior formation when the environment is brought to hydrate stable condition (Sloan and Koh, 2008).

There have been conflicting arguments in the literature concerning this curious phenomenon, however. One group of researchers suggests that the memory-effect is due to residual-structures of clathrate in the solution after the hydrate dissociation which leaves partial hydrate cages which leaves water structures within the system (Makogon, 1974; Chen, 1980). The other group, on the other hand, suggests that it is due to the dissolved gas remaining in the solution after the hydrate decomposition, which leads to concentrated hydrate forming gas within the solution and along with retarded diffusion, the hydrate is more readily formed (Rodger, 2000). Few molecular simulations were conducted to observe the phenomenon by other research groups but they also yielded

conflicting results as mentioned above (Sloan and Koh, 2008). So far, no systematic approach has been performed to gain insight into this phenomenon and predict its behavior.

It is also important to note that, as mentioned before, the hydrate dissociation is an endothermic process. This leads to a decrease in local temperature during the dissociation and creates an ideal condition for secondary gas hydrate or ice formation (Seol and Myshakin, 2011). Previous research suggested that ice-rind, Figure 6a, forming around the melting hydrate, Figure 6b, shifts the hydrate stability, requiring additional energy for dissociation and making gas release difficult (Stern, 2003).

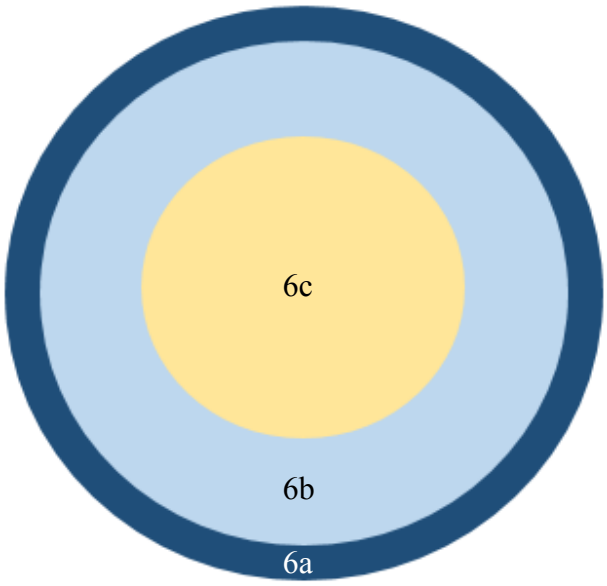

Figure 6: Ice-rind surrounding the melting hydrate. 6a: ice-rind, 6b: hydrate and 6c: soil

3.2 Experiment Preparations

The main objective of the research is to investigate the phase equilibria in water-methane system with structural memory-effect of water on hydrate re-formation in both free water and gas system and in pore-space. These phenomenon is further investigated in the next chapter using the Molecular Dynamics (MD) simulations.

All of the experimental studies were carried in laboratory room 721 at the Harold Vance Department of Petroleum Engineering. The experiments mainly consisted of utilizing the Thermotron's S-16C temperature controlled chamber, a high pressure cell, thermocouples, transducers and methane gas. The data acquisitions were done via National Instrument's NI cDAQ-9174 USB Chassis and NI9219 analog input module which transfers data to Labview for visualization and data storage. More thorough experimental apparatus details and methods will be discussed for each conducted experiments.

To visually see the hydrate formation and to observe the phenomenon in the simplest method possible, the phase equilibria studies in free water-gas system was conducted. This was done by using the previously fabricated high pressure stainless steel cell with six acrylic windows as shown in Figure 7 below, it was previously designed by Dr. Makogon.

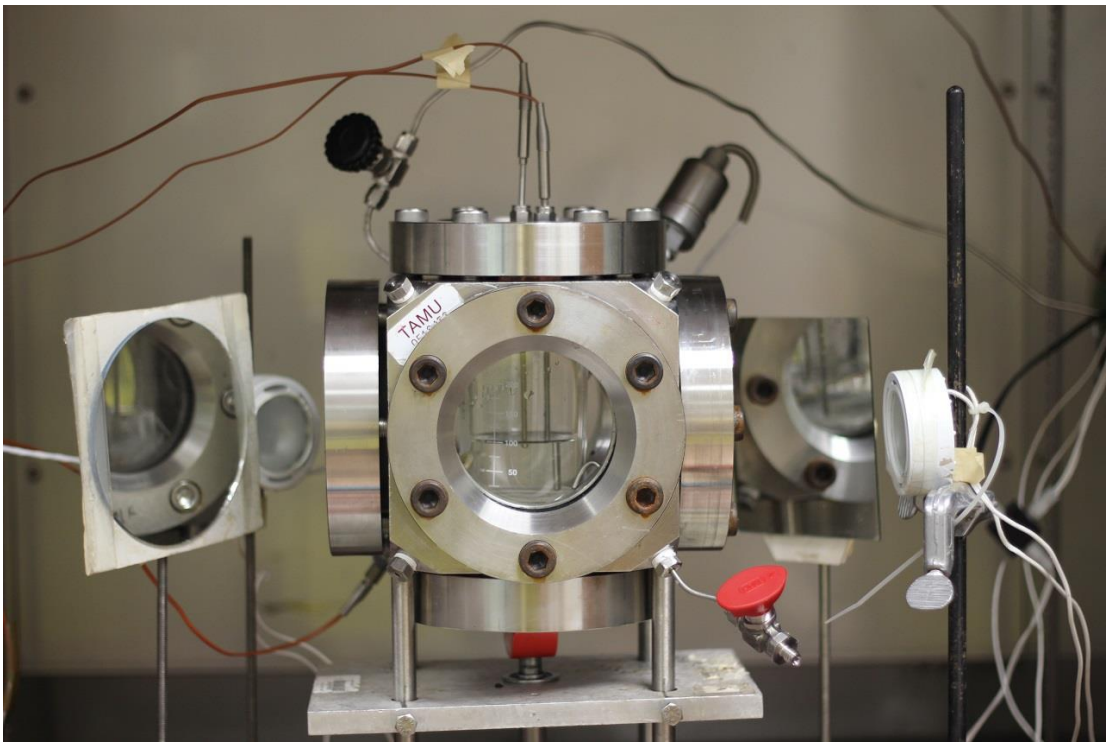

Figure 7: Apparatus setup inside of the temperature controlled chamber.

This experiment apparatus consisted of two CHROMEGA-ALOMEGA 304 Stainless Steel sheath grounded K-type thermocouples with 1/8inch radius, one near the water and gas contact, and the other submerged deep inside the water. One Full bridge PX906-7.5KGV transducer capable of measuring pressure up to 517 Bar (7500 Psi) and a methane gas tank to pressurize the stainless steel cell. Of the six windows surrounding the stainless steel cell, one window was replaced with a machined, lathed and threaded copper cylinder plug as shown in Figure 8 to better trigger hydrate formation and to accommodate two thermocouples. A simple sketch of the overall apparatus showing the different components and equipment is shown in Figure 9 below.

Figure 8: Manufactured copper cylinder to replace one of the acrylic windows and also to accommodate two thermocouples

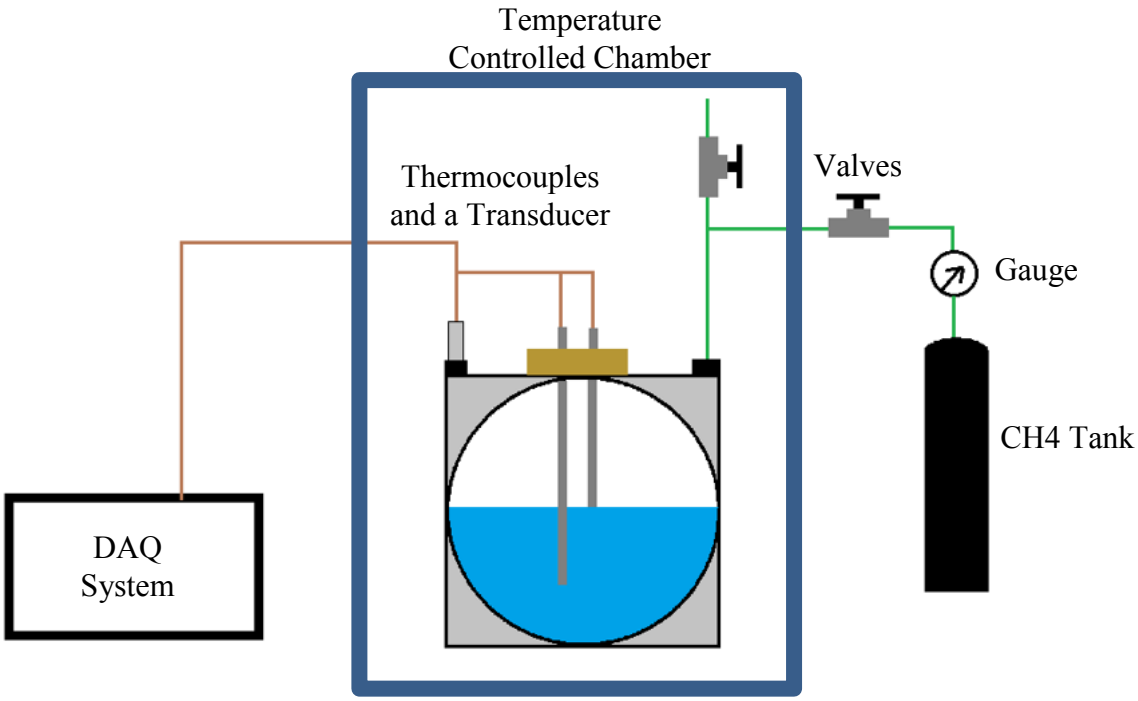

Figure 9: Simple schematics of the experiment

The prepared stainless steel cell with DAQ system and experimental equipment was filled halfway with filtered water at the room temperature. After the leak test, the stainless steel cell was pressurized with source gas to various pressure points. The entire apparatus was placed inside of the Thermotron's S-16C temperature controlled chamber to conduct experiments at various temperature points. The experiment was conducted under isochoric condition.

3.3 Preliminary Experiment and Preparation

Water is the single most influential hydrate former and understanding of water is very crucial in understanding hydrate formations. Since methane hydrate exhibits similar traits of structure *ih* ice, or ice 1, it was important to visually compare, observe and collect data for ice 1 formation first under the methane hydrate forming conditions but without forming hydrates.

Two sets of preliminary experiments were conducted at various pressure points, one involving a copper cylinder plug and one without it. Nitrogen was used to pressurize the cell. The preliminary experiments were also conducted to check the equipment calibration and to test the stainless steel cell leakage.

Onset of pressurized ice formation can be distinguished by a propagating solid-liquid front across the cell with most of the propagation finishing within 3 seconds or so. With copper cylinder plug placed right above the water, the propagation front initiated from the liquid-gas surface and ended at the bottom of the liquid as shown in Figure 10. This is due to high thermal conductivity of copper leading to localized low temperature

on the liquid-gas surface. The high thermal conductivity metal promotes heat transport thus leading to heat removal through the region where the copper cylinder is placed.

Without the copper cylinder, the propagation front initiated from the bottom of the liquid and propagated towards to liquid-gas surface as shown in Figure 11.

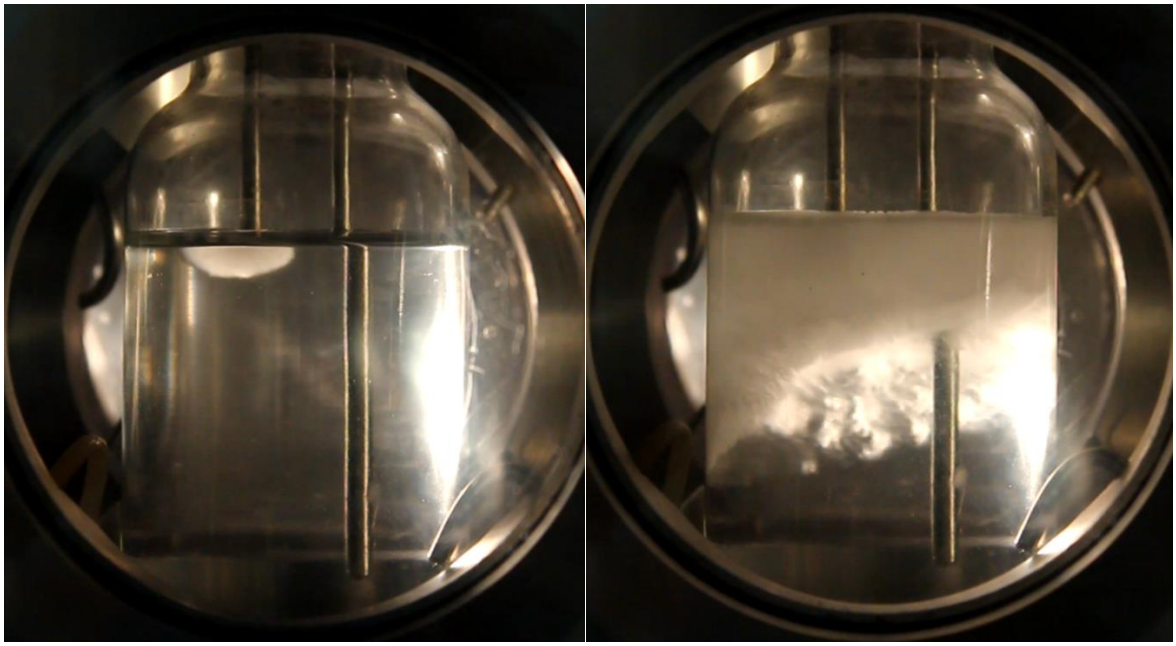

Figure 10: Ice propagating from ice-water interface towards the bottom

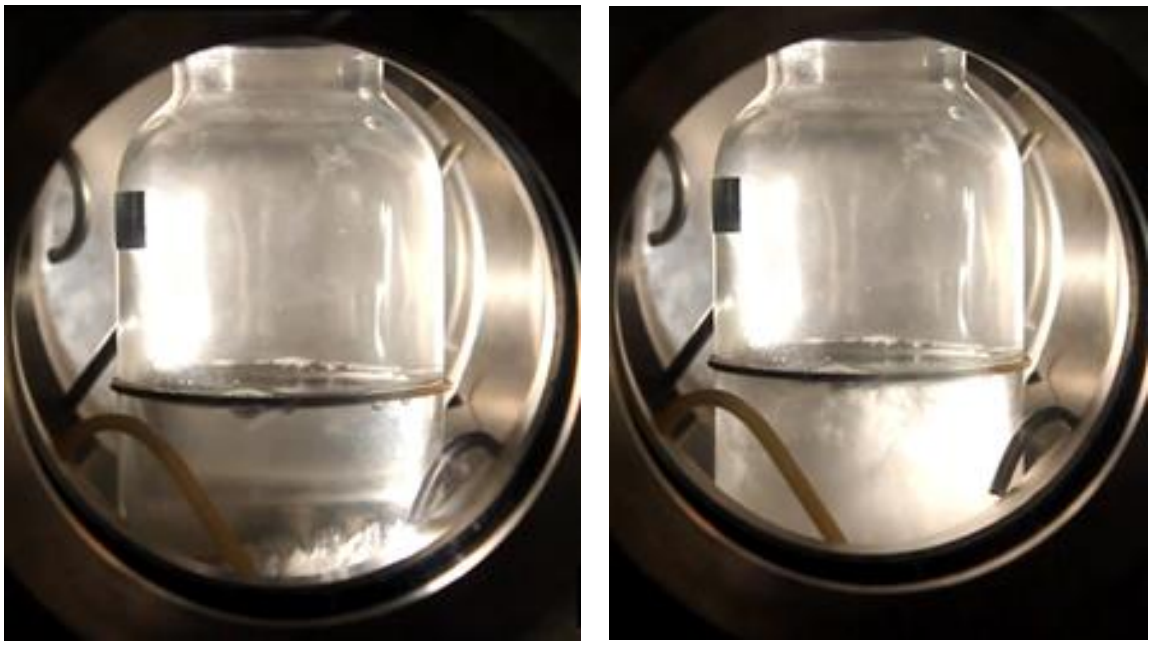

Figure 11: Ice propagation from the bottom towards the water-gas interface

The pressurized system also led to noticeable sub-cooling of liquid before triggering the ice propagation front. The results representing the onset temperature of ice formation are shown in Figure 12. It is also important to note that the presence of the copper cylinder plug also led to less sub-cooling, due to of copper cylinder contributing to localized low temperature on the liquid-gas surface.

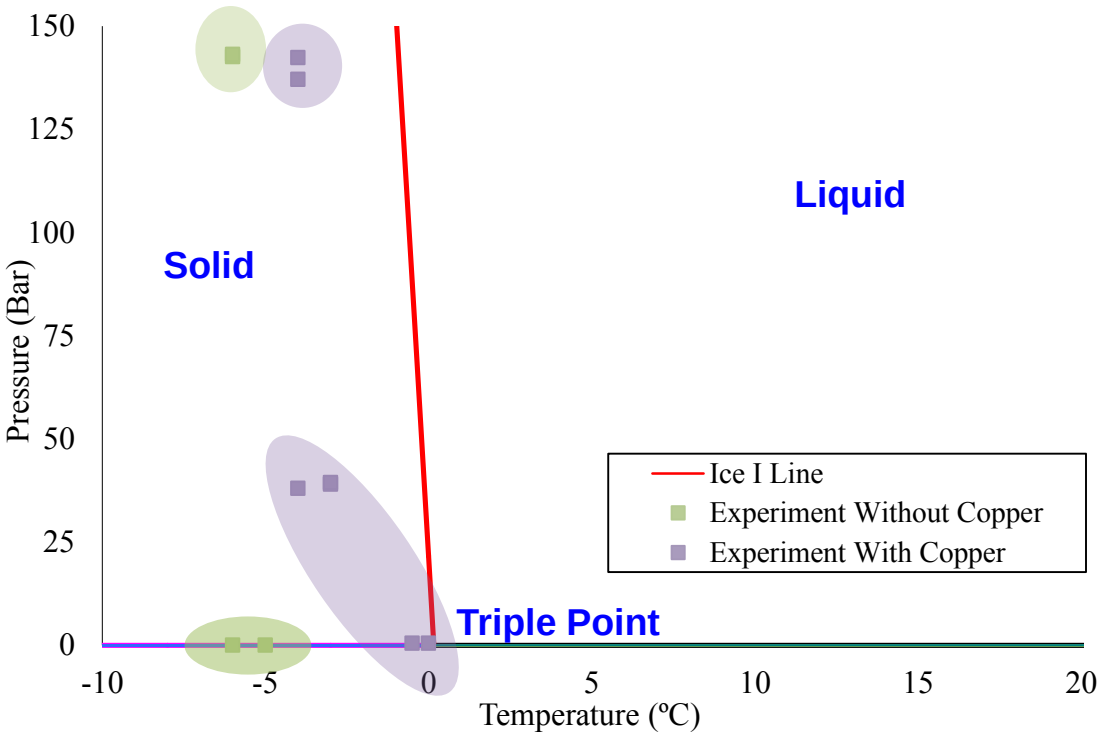

Figure 12: Experimental results from ice formation preliminary experiments

3.4 Hydrate Experiment

Two sets of experiments were conducted to study hydrate formation and its stability in free liquid-gas system. First experiment was conducted by placing the copper cylinder plug on the top of the stainless steel cell. Like the previous experiment with ice, the cell was pressurized by injecting the source gas, methane. The process and method of the experiment are otherwise very similar to preliminary ice experiments. A quick initial hydrate formation experiment showed that the hydrate formation is much slower process when compared with the ice formation. Compared to the ice formation propagation, which only takes few seconds to propagate, the hydrate propagation takes anywhere from hours to days. Figure 13 shows hydrate formation in the course of 24hours.

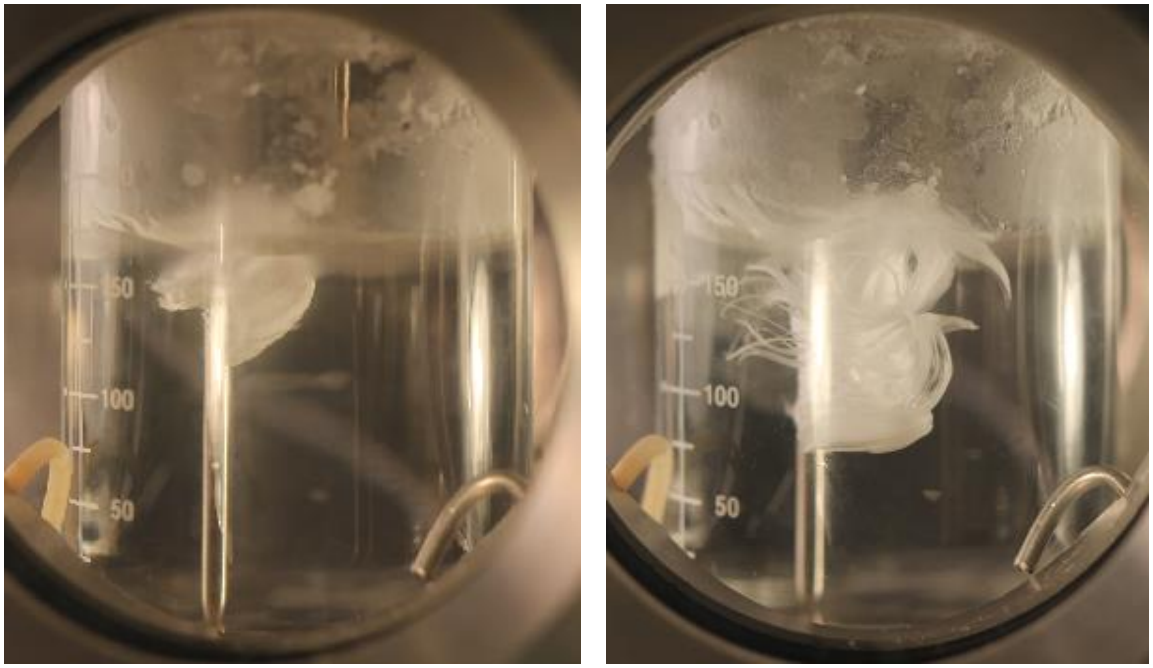

Figure 13: Methane hydrate formation in the course of 12 hours

The second sets of experiments of hydrate equilibria in water-gas system was conducted by placing copper cylinder plug on the rear window to the stainless steel cell. Likewise, the cell was pressurized with methane gas at various non-hydrate forming pressures and temperature points then the entire system was adjusted to hydrate forming condition to observe and collect data for methane hydrate equilibria for free water-gas system. The nucleation of hydrate formation was observed by video recording the experimental cell while acquiring data via DAQ system. For this experiment, only the nucleation temperature was recorded, then the system was left for at least 5 hours to continue hydrate formation. Nucleation of hydrate formation is shown in elipsoid in Figure 14 and formed hydrates after sufficient time is shown in Figure 15.

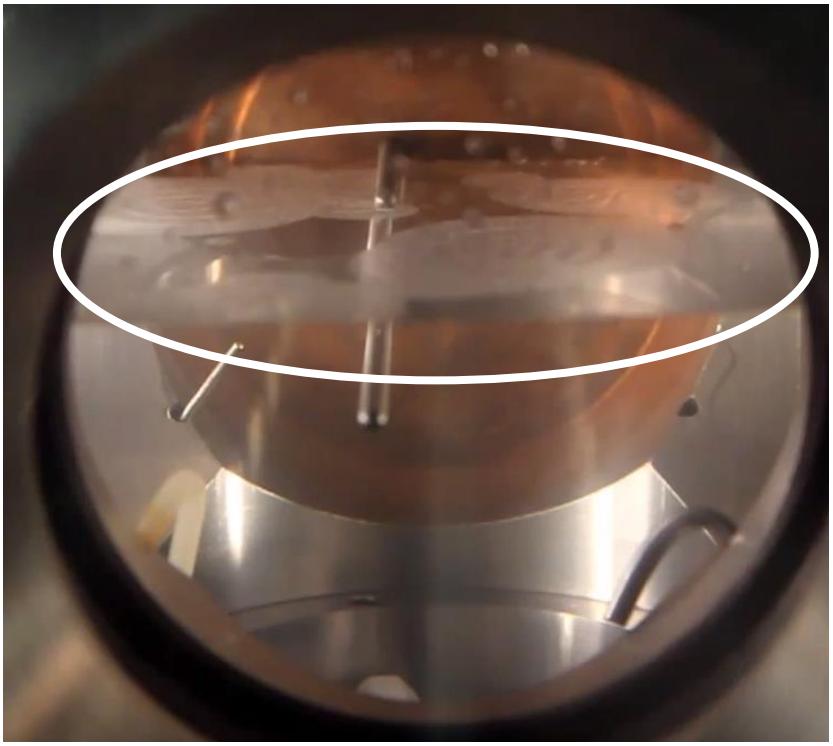

Figure 14: On set of methane hydrate nucleation

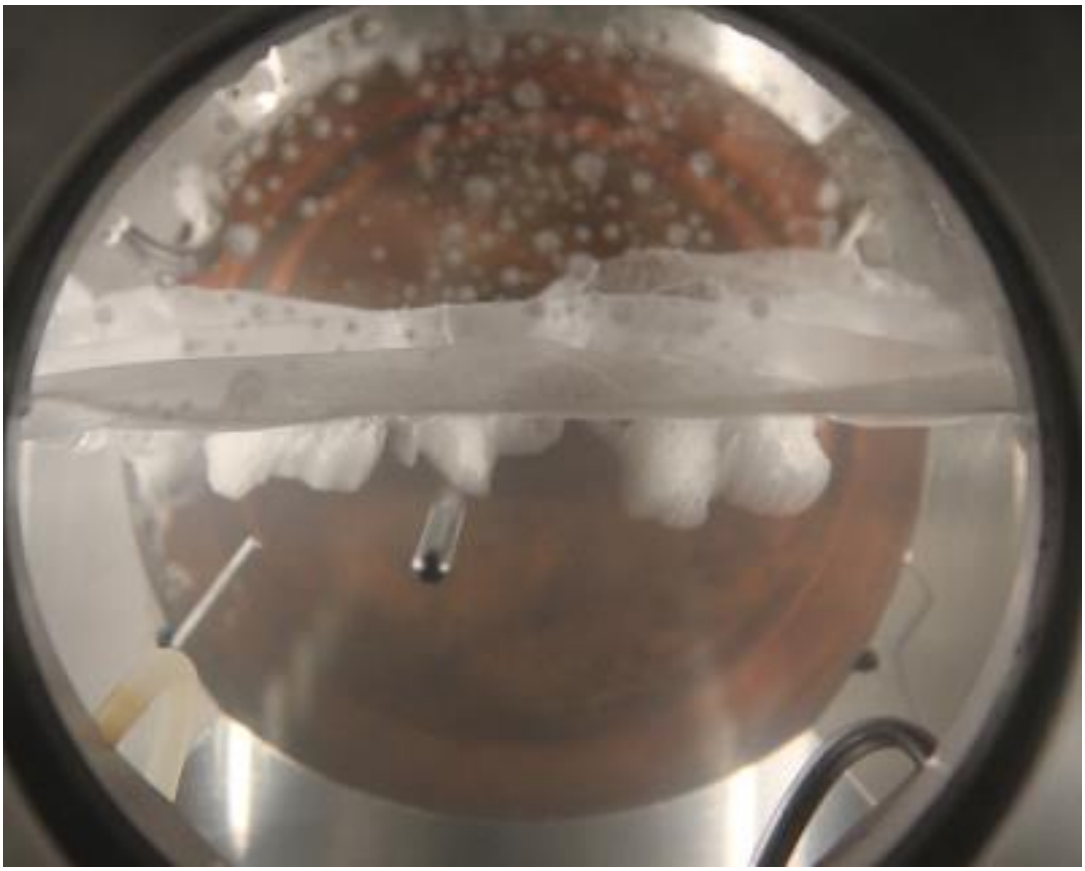

Figure 15: Methane hydrate after 5 hours of formation

After initial hydrate formation, the system was brought to non-hydrate forming condition to dissociate hydrates at various temperature points without changing the pressure. Then the system was brought to hydrate forming temperature again to investigate the structural memory-effect of water on hydrate re-formation.

3.5 Results and Discussions

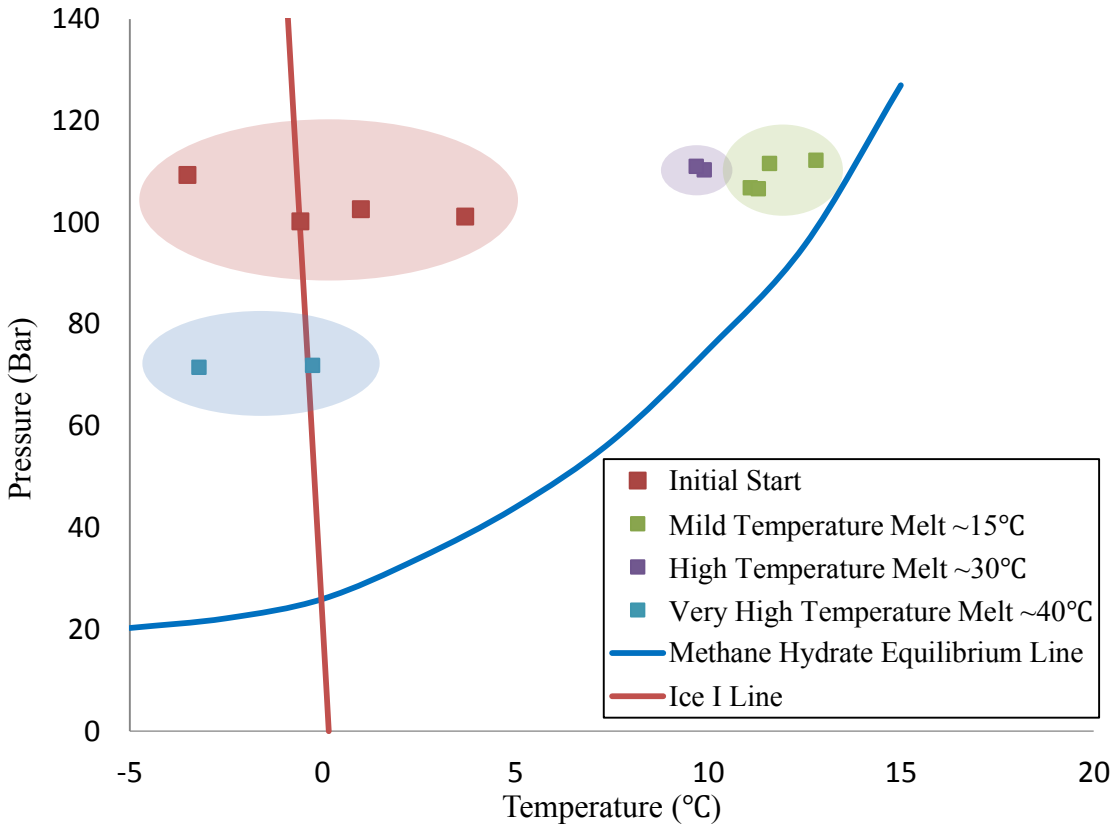

Figure 16: Experimental results showing the formation temperatures of methane hydrates in free water-gas interface

The summarized results for the experiments are shown in Figure 16. As in the case the ice formation experiments, the hydrate formation also requires sub-cooling below the methane-hydrate stable conditions of at least 10°C, noted in red cloud. However, the subsequent experiments of melting the hydrates in non-hydrate condition noted in green and purple clouds yielded much less sub-cooling when compared with initial hydrate formation. This indicates that the structual memory of water affects the hydrate re-formation. It can also be noted that by melting the hydrate in higher

temperature requires higher sub-cooling for subsequent hydrate formation. This is also an indication that even though the hydrates are kept in non-hydrate forming conditions or appears to be melted to human eyes, there are still invisible hydrate seeds within the fluid which will readily trigger the subsequent hydrate formation. From the experimental result, it has been found that the hydrate seeds could disappear, or destroyed, when the system is carried to a very high temperature of 40℃ along with little depresssurization.

The compiled experimental results of methane hydrate formation temperatures in Figure 16 suggests that the methane hydrates retain invisible seeds of structural memory of water which will affect re-formation by triggering the formation more readily if it was melted to mild temperature up to 30 ℃. This identified structural memory seeds of water are destroyed or disappears when the hydrates are melted to temperature beyond 40℃.

CHAPTER IV

MOLECULAR DYNAMIC SIMULATION OF METHANE AND WATER SYSTEM

4.1 Simulation Approach

To observe and study the effect of hydrogen bonds in hydrate formation, a series of molecular dynamic (MD) simulations have been conducted. For the following research, the software known as GROningen MAchine for Chemical Simulations (GROMACS) Version 3.6.4 was used to research the hydrogen bonding of methane hydrates in molecular level. The simulations were run through Texas A&M's Supercomputing system.

There are various ways to conduct molecular level simulations using the water molecules. Currently there are more than 40 recognized water models and most of the models are created for only specific purpose, i.e. a water model established for freezing point prediction most likely is not going to represent the effect of vapor pressure correctly. Depending on the purpose, there are few ways to model water molecules for MD simulations as shown in Figure 17. Most well-known water models includes SPC, SPC/E, TIP3P and TIP4P water models.

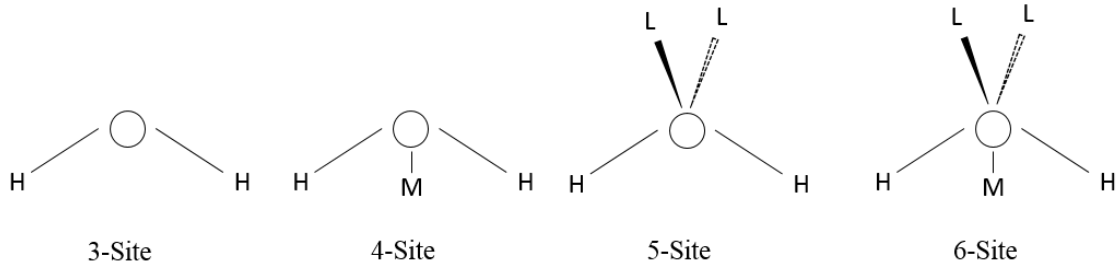

Figure 17: Four well known methods in modeling water molecules for MD simulation, where H represents Hydrogen, O represents Oxygen, L represents a lone pair for non-interacting valence electron and M represents a dummy atom to improve electrostatic distribution.

Like the conducted experiments, few preliminary simulations were conducted to determine parameters and simulation inputs. Choosing the correct water model is very crucial as very crude water model, i.e. SPC model, would not give accurate results for the hydrate simulation but a very meticulous water model will take anywhere from few weeks to few months of computational time to give a meaningful results. Hence, few simple water simulations were conducted to determine which water model to use and which water models to discard. After comparing SPCE, TIP3P, TIP4P and TIP5P water models, it was determined that TIP4P gives most meaning result for the current research. (Koh, 2013) With a personal advice from Dr. Koh from Colorado School of Mines, TIP4P/ICE (a variance of TIP4P) was used for the MD Simulations. The model can simulate the hydrogen bonding associated with the hydrate formation and re-formation.

For the MD simulation, within a simulation box of 4.8nm x 4.8nm x 4.8nm with periodic boundary condition, a 64 repeating unit cells of methane hydrates were created. A unit cell is a simplest repeating unit in a crystal and a unit cell of methane hydrate is

composed to 46 water molecules and 8 sites for methane molecules as shown in Figure 18.

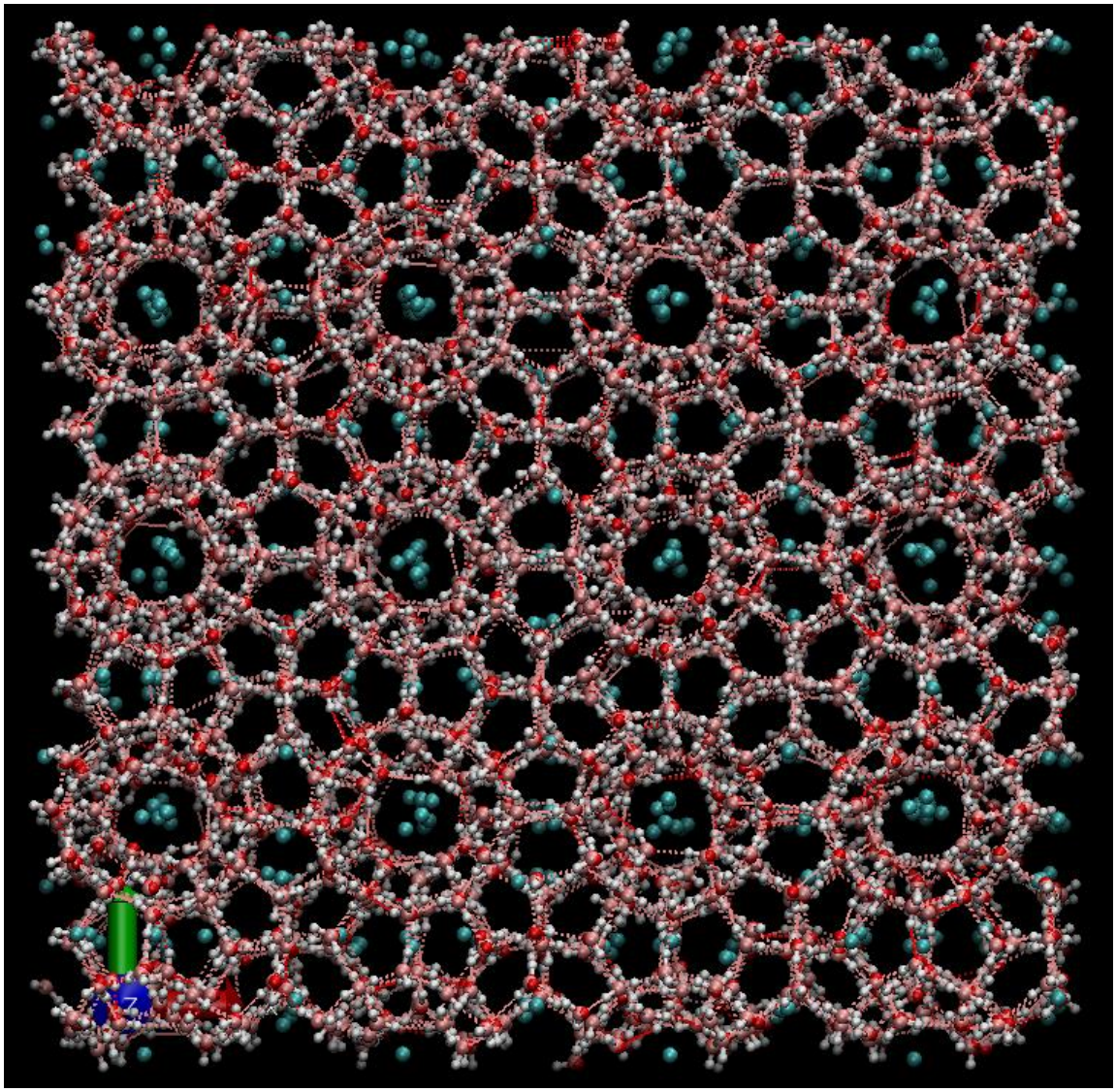

Figure 18: Simulation input box consisting methane hydrates with 64 repeating unit cells

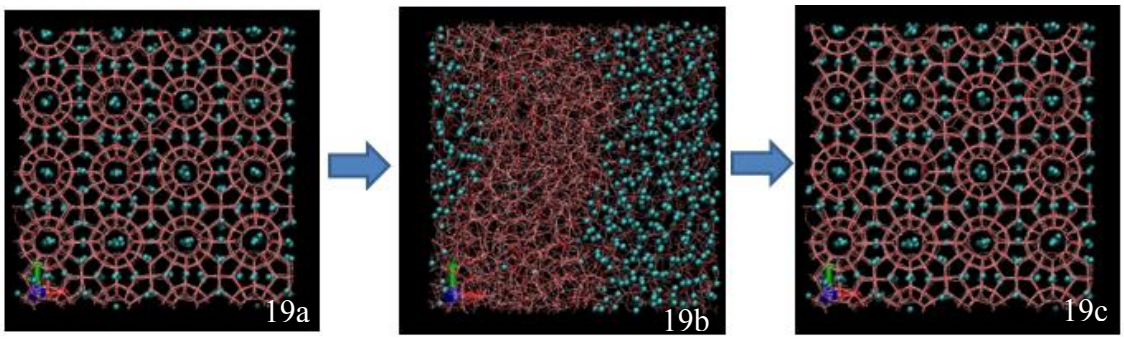

Figure 19: Ideal, yet very time consuming approach for running simulation

TIP4P/ICE water molecule model was used and a methane was represented as a simple atom. The Optimized Potentials for Liquid Simulation All-Atom force field, OPLS/AA, was used. To ensure hydrate structure, simulation box in Figure 18 was simulated in 250 Kelvin (-23.15℃ or -9.67 F) and 500 bar (7252 psi) for at least 20 nanoseconds.

Initially, the formed hydrates in simulation box, Figure 19a, was to be melted like shown in Figure 19b, and then re-formed like shown in Figure 19c. However, this approach could take minimum of few weeks to few months to obtain any meaning result.

To conduct the research in timely manner, a rule known as the Lindemann's criterion was used to determine the melting of simulated methane hydrates. In 1910, Frederick Lindemann proposed that the melting of a solid structure occurs when the mean amplitudes or displacements of particles, $< u^2 >^{\frac{1}{2}}$, in a crystal structure reaches some characteristic length L with respect to its nearest neighbor in a distance R_o. This relationship is shown in Equation 1. Lindemann originally proposed the characteristic value to be 0.5 to conclude the melting occurred, but over the course of time, various

researchers determined that the value of L is 0.113 for body centered cubic structures, i.e.alkali metals, 0.071 for face centered cubic structures, i.e. aluminum, copper, gold etc. (Stillinger and Weber, 1980) or 0.15 for typical liquid structures. (Hansen and McDonald, 2006)

$$L = \frac{<u^2>^{\frac{1}{2}}}{R_0} \quad \cdots\cdots (1)$$

Where $< u^2 >^{\frac{1}{2}}$ is the average mean displacement of the molecules, R_0 is distance to the molecule's nearest neighbor. Here we considered that when the L reaches 0.15, the molecule can be considered as melted.

The analysis of the simulation output cannot be done over the entire molecules. This is because there are 64 repeating unit cells, which is consisted of 2944 water molecules and 512 methane molecules. The periodic boundary condition of the simulation input box will also lead to outliers in displacement calculation of the molecules as one end of the molecule may appear from the other end, leading the significant error in determining Lindemann's number. Because of these reasons, a Representative Elementary Volume (REV) was used is introduced.

The REV is the smallest volume which can represent the whole sample as long as the chosen, representative sample contains a sufficient number of inclusions to be a representative model. In the case of periodic material, a unit cell can be used as smallest representative volume. (Hill, 1963) For the Lindemann's number determination, one unit cell of the methane hydrates and various random molecules, which are not affected by

the periodic boundary condition, were chosen for the Lindemann's characteristic number calculation. Only the oxygen atoms were considered in the calculations due to its large center of mass. Therefore displacements of the water molecules were calculated by observing the displacements of oxygen molecules.

The simulations were conducted by heating the simulation box to four temperatures of 293K (20℃ or 68F), 313k (40℃ or 104°F), 343K (70℃ or 158°F) and 373K (100℃ or 212°F) in canonical ensemble, NVT.

4.2 Results and Discussions

To emulate the experimental condition, MD simulations were done by changing the temperature values only. From the simulation results, shown in Figure 20, it was determined that the times at which the Lindemann's characteristic number reached 0.15 at various temperature points are: 50 nanoseconds for 293K, 25 nanoseconds for 313K, 6 nanoseconds for 343K and 8.5 nanoseconds for 373K. Even though the melting of methane hydrate at 313K occurred earlier than the 343K, as the melting occurred, 343K simulation resulted in exponentially quicker melting.

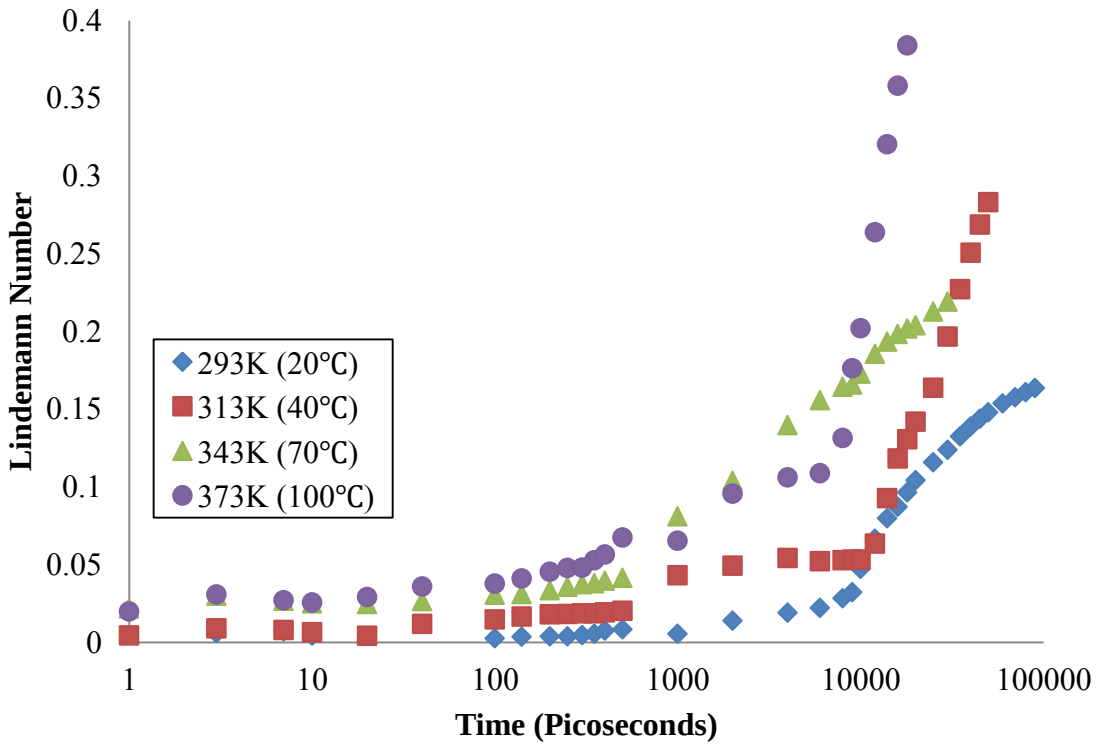

Figure 20: Simulation result in determining Lindemann Number

It has also been determined that from the simulation, the number of hydrogen bonds depends on the temperature of the system as shown in Figure 21. It can be determined that the heating temperature affects the stability of the hydrogen bonds. This suggest that by melting the hydrate at moderate temperature could leave hydrogen bond residues or seeds within the liquid crystals which behaves like melted methane hydrate system that are invisible to human eyes. Therefore, moderately melted methane hydrates leads to hydrogen bond residues and structural memory of water in the system, thus promoting the hydrate re-formation.

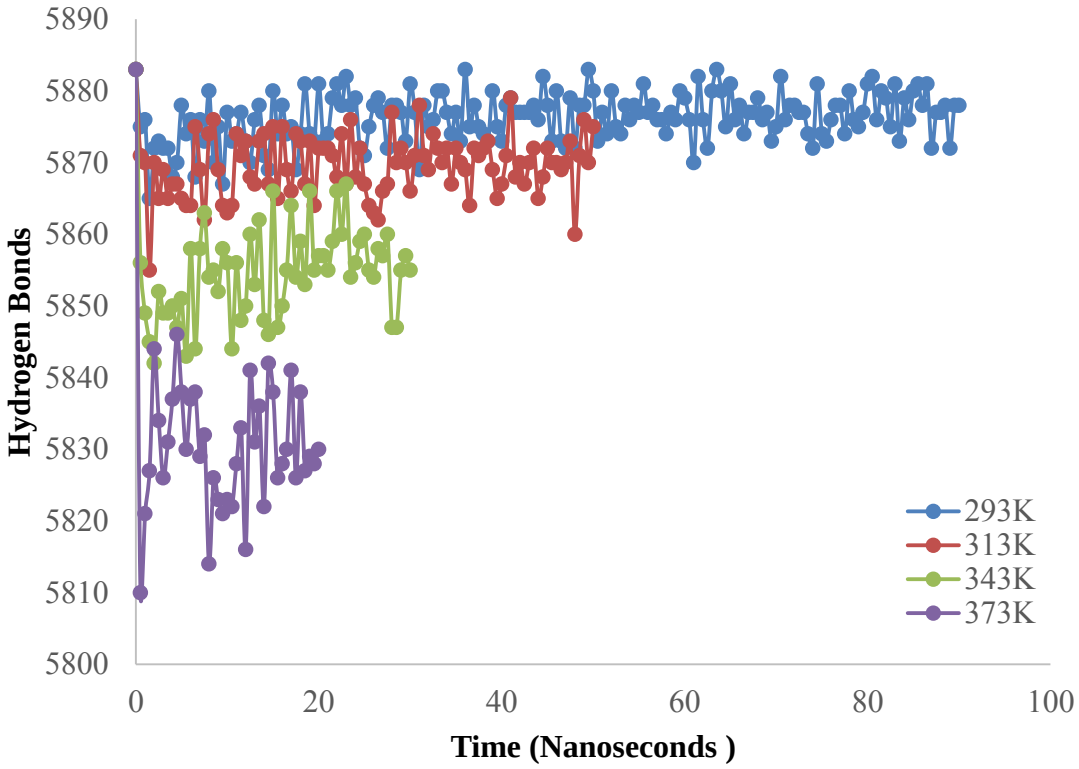

Figure 21: Change in number of hydrogen bonds in the system by different temperatures over simulation time

CHAPTER V

PHASE EQUILIBRIA IN PORE-SPACE

The phase equilibria studies in pore-space was conducted using the previously fabricated high pressure stainless steel cylinder as shown in Figure 22 below, this also was previously designed by Dr. Makogon. However to accommodate thermocouples and pressure transducer, a copper plug had to be designed and machined from a copper cylinder in the lab as shown in Figure 23.

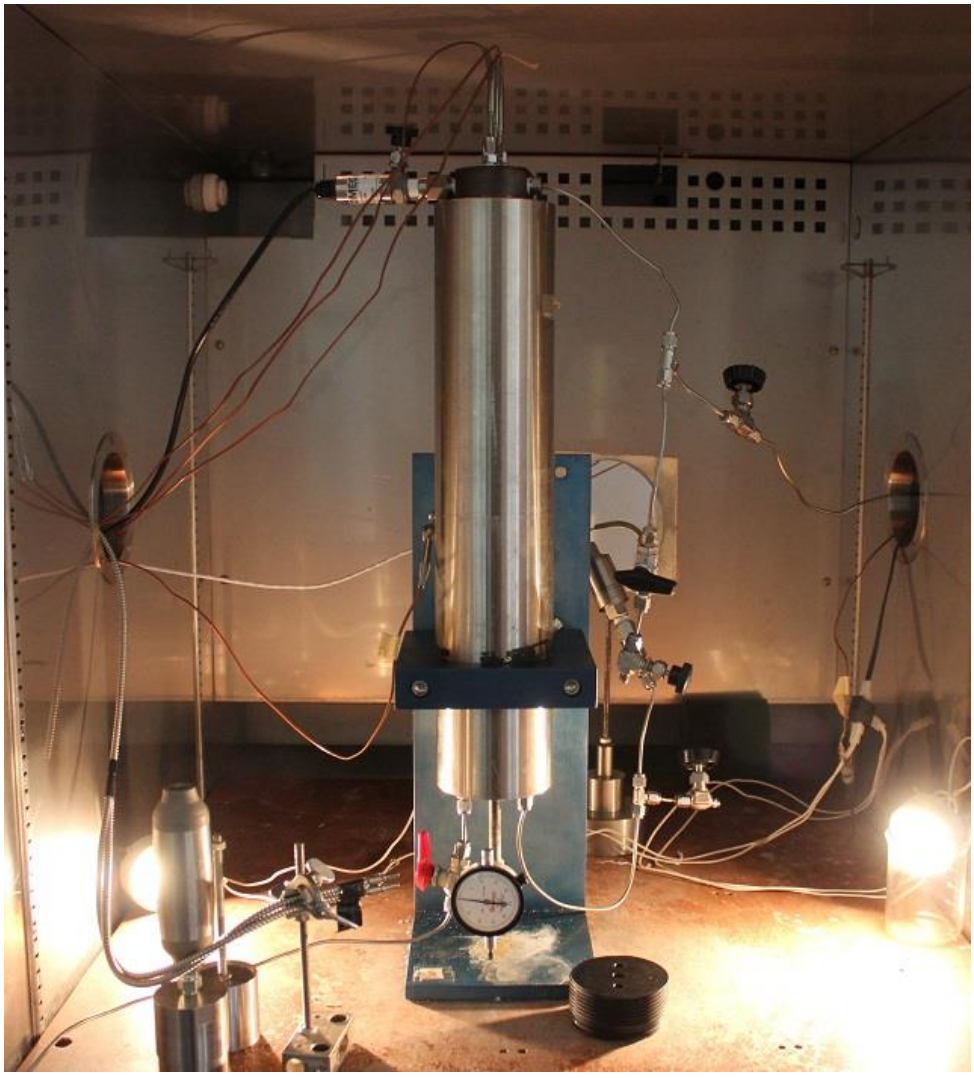

Figure 22: Apparatus setup for methane hydrate stability study in pore-space

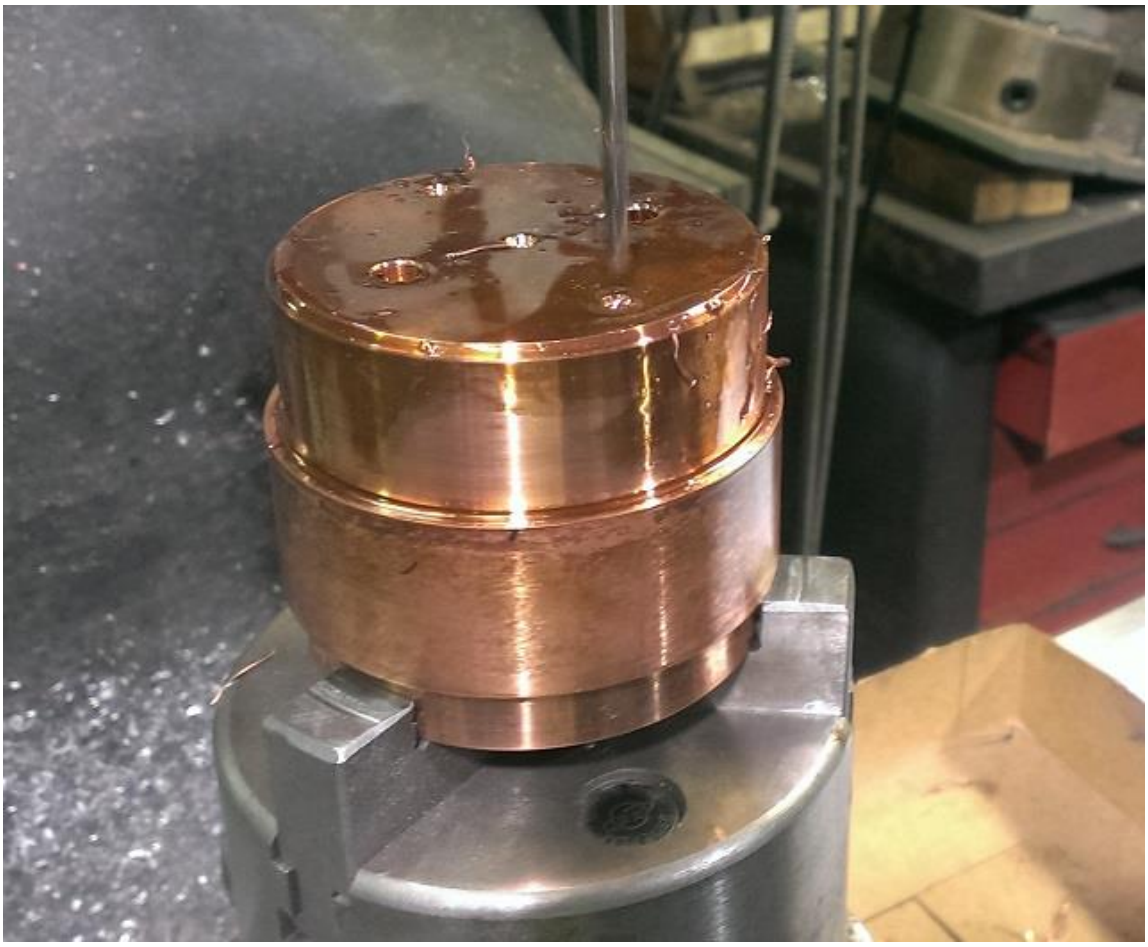

Figure 23: Machined Copper cylinder plug to accommodate three thermocouples, one transducer, and two ports for gas injection and removal

5.1 Preparation

As shown in the dissected diagram along with the dimensions and the sizes of the parts in Figure 24, the cylinder was divided into two main sections. Section A, the pore-space, and Section B, empty-space filled with water. This experiment apparatus consisted of three CHROMEGA-ALOMEGA 304 Stainless Steel sheath grounded K-type thermocouples with 1/8inch radius in section A. Locations and lengths of the thermocouples are also shown Figure 24. One Full bridge Omega PX906-7.5KGV

transducer capable of measuring pressure up to 517 Bar (7500 Psi) was placed between two plugs in Section B as shown in Figure 24 and a Omega PX309-100G5V transducer capable of measuring pressure up to 344 Bar (5000Psi) was used to measure pressure in Section A (Pore-space). Like the previous experiments, methane gas tank was used to pressurize the stainless steel cylinder. A simple schematics for the experiment is shown in Figure 25. Beads sands (quartz) were used for the experiment. The sieve analysis of the quartz sand is shown in Figure 26.

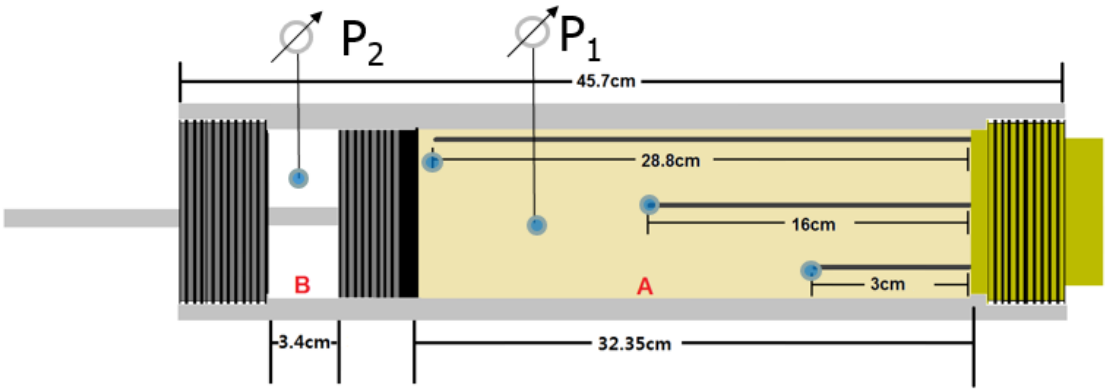

Figure 24: Dissected diagram of the stainless steel cylinder

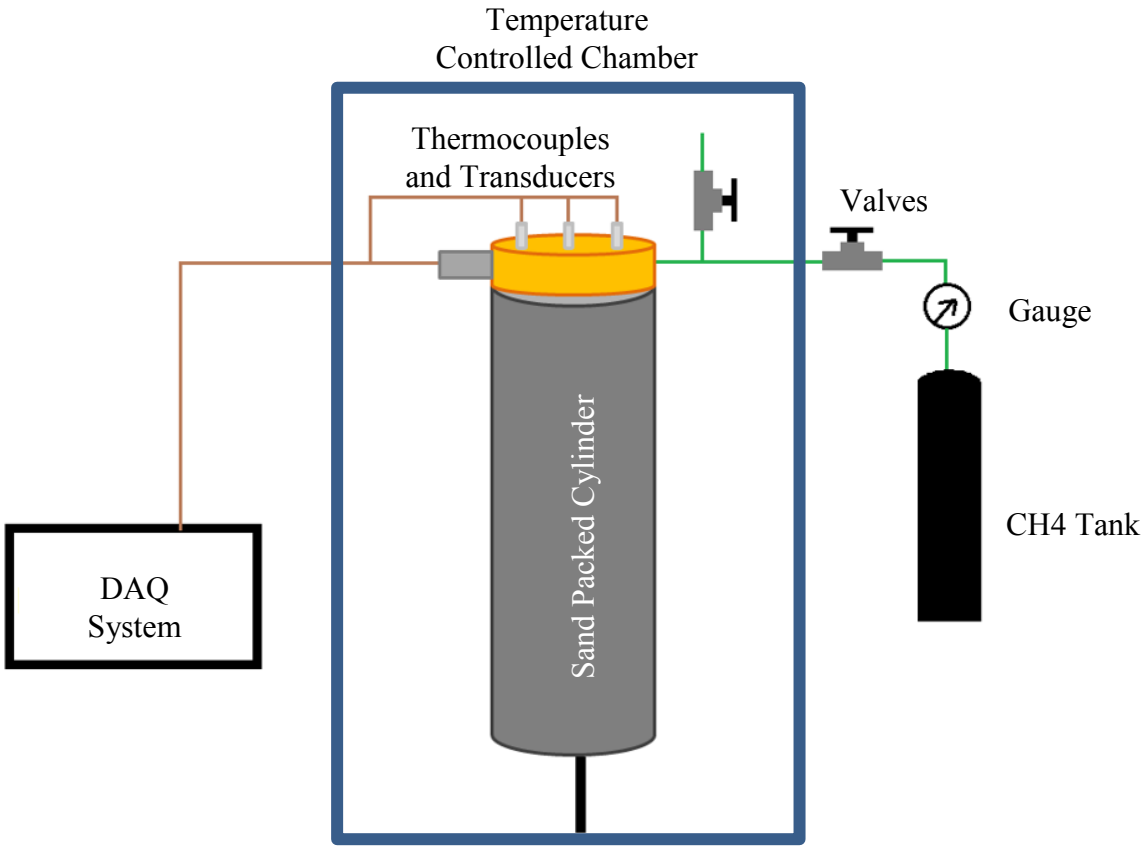

Figure 25: Simple schematic for the methane hydrate formation in pore-space experiment

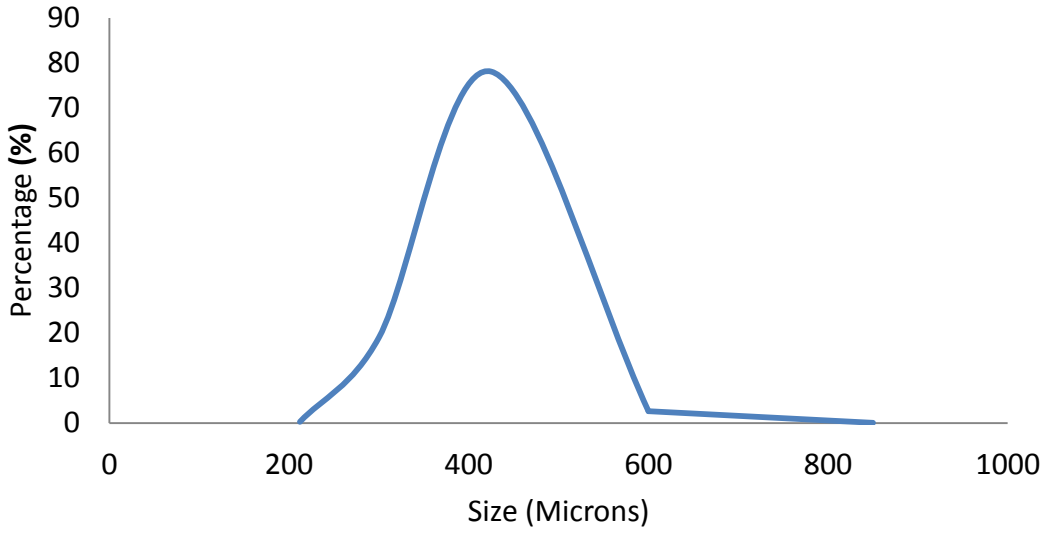

Figure 26: Sieve analysis of beads sands (quartz) that was used for the experiment

For the experiment, 1,200cm^3 of sands with porosity of 36.2%, determined by the water saturation method, was saturated 50% with filtered water. Thus using the partial saturation method for hydrate formation. Experimental sands were packed into the cylinder in Section A. Methane gas was then injected and flushed twice around 100 bar (about 18,500 scm^3 of methane injection in 217.2cm^3 pore-space) to remove air inside of the cylinder. After flushing the pore-volume, the cylinder was pressurized with methane to 103 bar in the Section A. Then the sands in cylinder was tight packed by pumping the water into Section B up to the pressure of 300 bar using the water pump until the piston separating the Section A and B stopped displacing. Thus the pore volume in Section A is 50% saturated with water and 50% filled with methane gas. Like the previous experiments, the following sets of experiments were conducted in isochoric condition with just temperature being the only parameter that was controlled.

Like the previous experiments, the following experiments were conducted by cooling the cylinder to hydrate forming condition to observe and determine the onset of hydrate formation. Since the stainless steel cylinder does not have any visible windows, the hydrate formation was noted by the exothermic reaction of hydrate formation leading the localized temperature increase on the thermocouples. Unlike the experiments conducted in free water-gas system, the entire experiment was conducted without changing initial input pressure, meaning no depressurization was done.

The experiments were conducted by first pressurizing the cylinder with water saturated sands to 103 bar at a room temperature, then the temperature controlled chamber was cooled to 1℃, a hydrate forming temperature without triggering the ice

formation. Then the system was kept in 1℃ for at least 12 hours to complete hydrate formation. Then the system was heated to non-hydrate forming temperature to melt the hydrates in the system. Subsequent experiments and the results have been conducted by only changing the temperature. After completing one complete experimental cycle, the results from collected data have been plotted on pressure-temperature graph to determine the onset temperature of methane hydrate formation.

5.2 Results and Discussions

The Figure 27 shows the course of the experiment by plotting the pressure against the temperature from the initial condition to the final condition. The stainless steel cylinder was initially pressurized at a room temperature of 25.3 ℃ at 103.54bar (Point A in Figure 27). Then the system was cooled to 1 ℃ (Point B in Figure 27) to trigger hydrate formation and kept for at least 12 hours (Point C in Figure 27). Then the system was heated to hydrate dissociation condition of 17 ℃, 25 ℃, 35 ℃ and 40 ℃ for another minimum of 12 hours (Point D in Figure 27). Then the procedures were repeated to determine initial hydrate forming temperature.

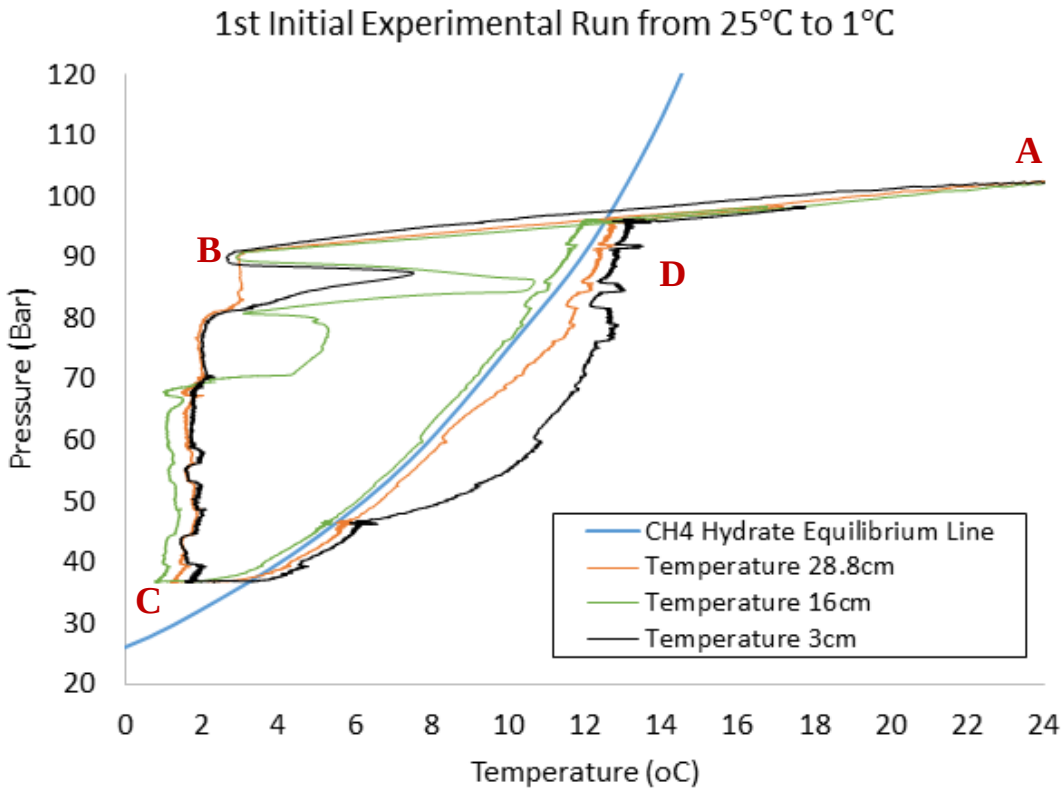

Figure 27: Initial experimental result of the hydrate formation study in pore-space with three different lines representing the data collected from three different locations

The established methane hydrate stability line (Makogon, 1997) is shown in blue to compare how the experimental results compare with the theoretical stability line. From the initial experiment, the first hydrate formation occurred at point B at 2.84℃, more than a 9.16℃ sub-cooling. As shown in the Figure 27, there is an evident temperature jump in the system due to the exothermic process of hydrate formation releasing the heat at point B.

The system at point C is then heated to 17℃, point D, and kept for at least 12 hours to ensure that all hydrates have been melted. From the Figure 28, it is shown that

during the dissociation process, the thermocouple located in 16cm, or about halfway from the one end of the cylinder closely follows the theoretical methane hydrate curve when compared with thermocouples located in 28.8cm and 3cm. This is an indication that the most hydrates are concentrated in the center of the cylinder.

After keeping the system at 17℃ for sufficient time at point D, the experimental system was cooled to 1℃, Point F, again to initiate hydrate formation. From the Figure 28, it is shown that the very first onset of hydrate formation for this experiment occurred at 8.71℃, point E. This 3.29℃ sub-cooling and is much less than the 9.16℃ sub-cooling of initial hydrate formation. This 5.87℃ difference is the evidence that the structural memory of water is present in the system. After keeping the system to 1℃ for more than

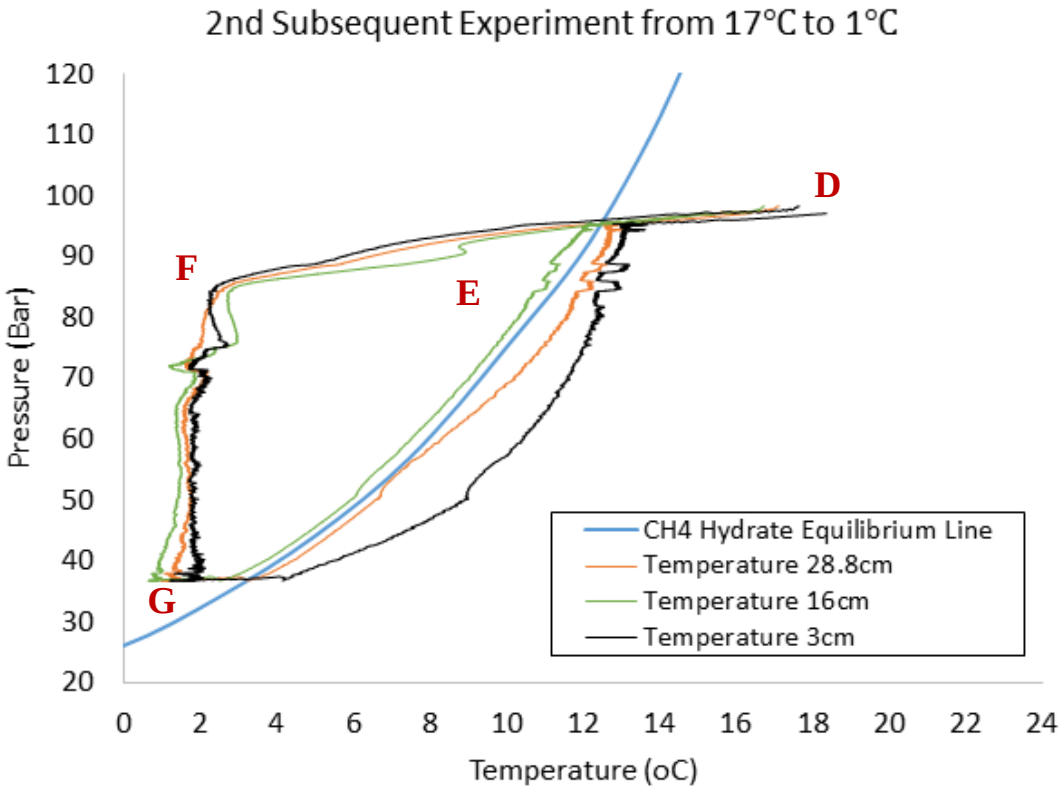

Figure 28: Result of the 2nd subsequent experiment by melting system to 17℃

12 hours, point G, to completely form hydrates, the experimental setup was heated to near room temperature of 25℃, point H, as shown in Figure 29.

Cooling the system from 25℃, point H, to 1℃, point J, also led to lower sub-cooling and hydrate formation temperature of 8.32℃, point I. This is comparable to hydrate formation temperature when the system was cooled from 17℃.

Repeating the process and heating the system to 35℃, point K (Entire x-axis is not shown to keep the graph in same scale as the previous graphs) did not significantly alter the subsequent hydrate formation temperature, which led to hydrate formation at 8.49℃, point L. Thus indicating that the hydrate seeds are still present in the system even when the system was heated to 35℃ as shown in Figure 30.

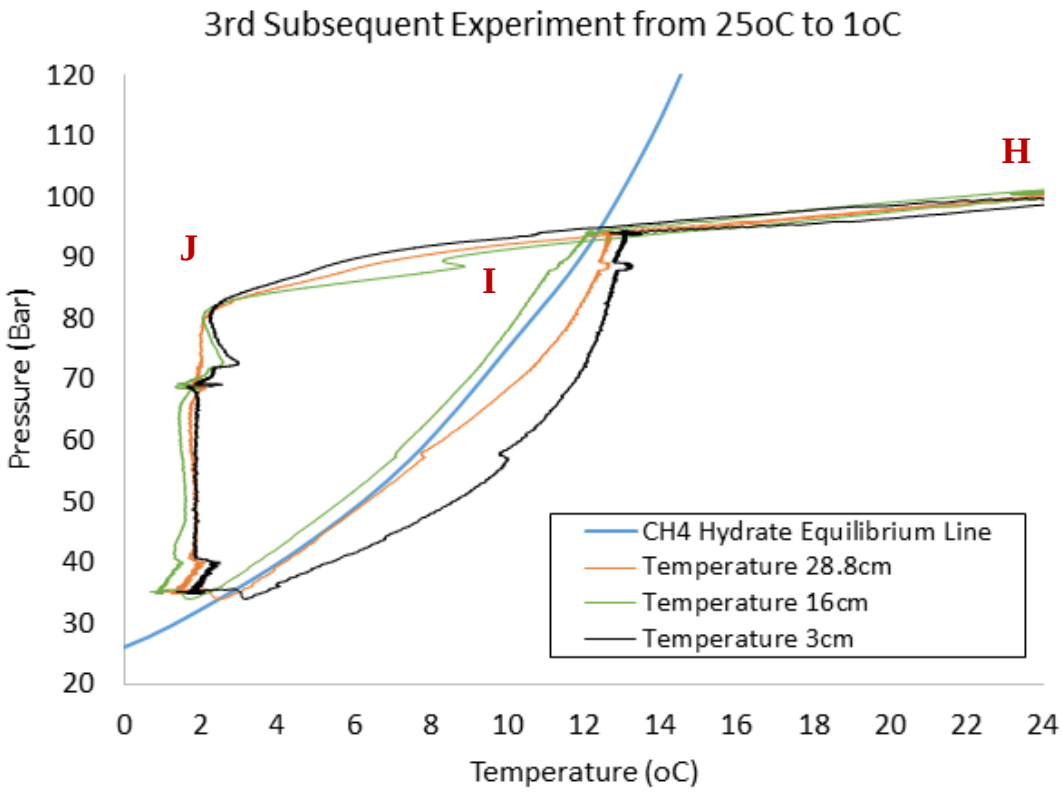

Figure 29: Result of the 3rd subsequent experiment by melting system to 25℃

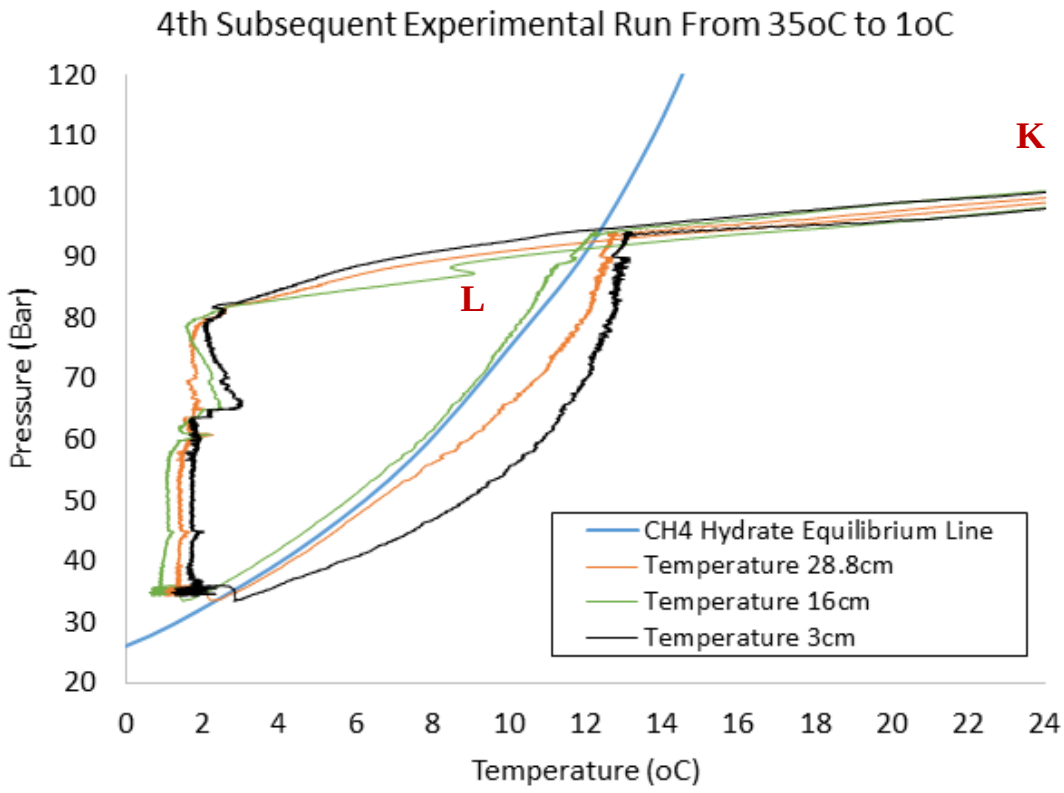

Figure 30: Result of the 4th subsequent experiment by melting system to 35℃

It was only after heating the system to 40℃, Point M, that the apparent structural memory of water was completely destroyed, Point N. The experimental data suggest that the system was reverted back to the initial condition when the system was heated to 40℃ as shown in Figure 31.

After heating the system to 40℃, the onset of hydrate formation occurred at the temperature of 3.4℃, Point N. This value is very similar to initial hydrate forming temperature of 2.84℃, Point B in Figure 27.

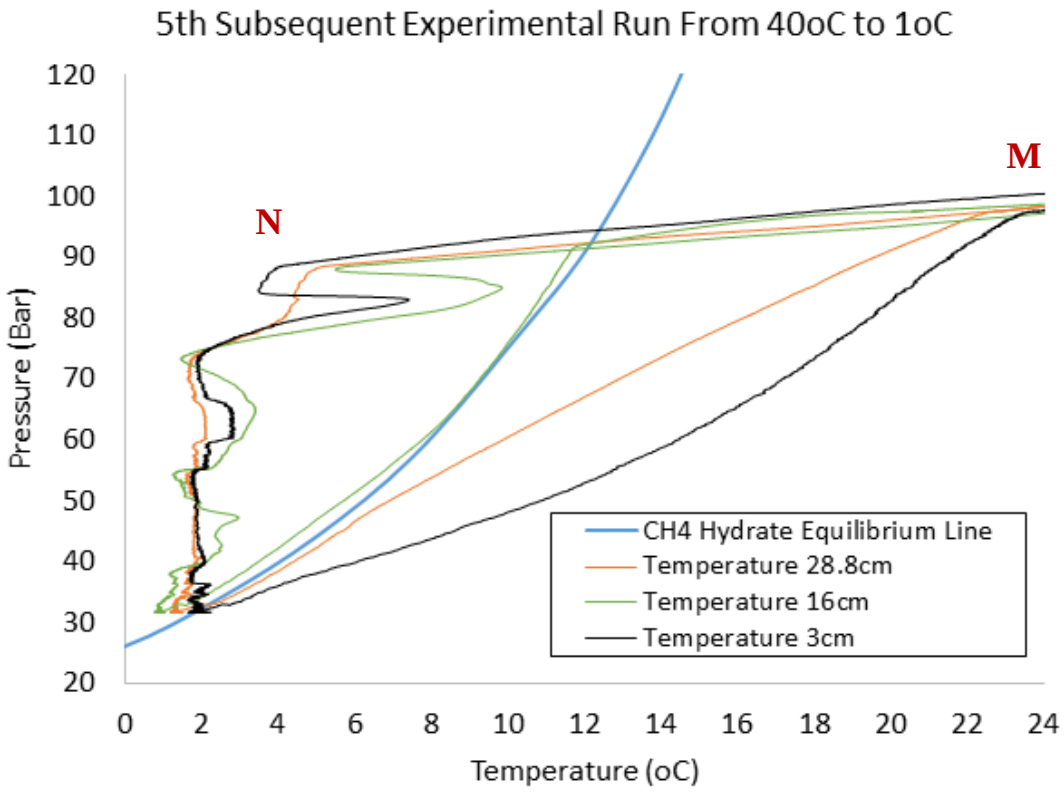

Figure 31: Result of the 5th subsequent experiment by melting system to 40℃

Thus this experiment suggests that it is by heating the hydrate system to 40℃ that will destroy hydrate seeds in the system that will no longer exhibit a memory-effect within the liquid to ensure tougher condition for formation again, when compared with mildly dissociating the methane hydrates. The summarized table of the experimental results are shown in Table 1.

	Experiment Initial Temperature	Hydrate Formation Temperature	Sub-Cooling Temperature
Initial Formation	25℃	2.84℃	9.16℃
2nd Subsequent Experiment	17℃	8.71℃	3.29℃
3rd Subsequent Experiment	25℃	8.32℃	3.68℃
4th Subsequent Experiment	35℃	8.49℃	3.51℃
5th Subsequent Experiment	40℃	3.40℃	8.60℃

Table 1: Summarized experimental results

CHAPTER VI

CONCLUSIONS AND SUGGESTIONS

In this research two series of experiments along with a MD simulation was conducted to examine the structural memory-effect of water on hydrate re-formation. The methane was introduced to a system with just water and another in water saturated pore network. From the room temperature, the pressurized experimental system was cooled to hydrate stable condition, then melted to various hydrate dissociating temperature under isochoric condition to collect data on onset of hydrate forming temperature. The MD simulation was conducted in canonical ensemble, NVT by first stabilizing methane hydrate structure then melting it by controlling the temperature. Through this research, the following conclusions have been made

- When solid methane hydrates melt at moderate temperature, the melted liquid solution retains a memory-effect.
- The system with previous hydrate history will lost its memory-effect if the system is heated sufficiently to 40℃. This shall be useful for flow assurance problems associated with hydrate plugs.
- The hydrogen bond is dependent on the temperature, thus higher temperature destroys more hydrogen bonds, thus effectively destroying the hydrate cage.

There are few suggestion for the future research relating to this memory-effect phenomenon.

- This phenomenon shall also be studied by using the depressurizing the system to hydrate melting pressure, instead of just changing the temperature.
- Perhaps keep the system in moderate hydrate melting temperature of below 40℃ for much longer time, perhaps for few days or weeks.
- Conduct MD simulations without Lindemann's criterion and run the simulation for extended periods of time.

REFERENCES

Berge, L. I., K. A. Jacobsen, and A. Solstad (1999), Measured acoustic wave velocities of R11(CCl3F) hydrate samples with and without sand as a function of hydrate concentration, J. Geophys. Res., 104, 15,415–15,424

Bohrmann, G., J. Greinert, E. Suess, and M. Torres (1998), Authigenic carbonates from the Cascadia subduction zone and their relation to gas hydrate stability, Geology, 26, 647 – 650, doi:10.1130/0091-7613(1998)026<0647:ACFTCS>2.3.CO;2

Buffett, B., and O. Zatsepina (2000), Formation of gas hydrate from dissolved gas in natural porous media, Mar. Geol., 164, 69–77

Chen, T.S., A Molecular Dynamics Study of the Stability of Small Pre-nucleation Water Clusters, (1980) Dissertation, U. Missouri-Rolla, University Microfilms No. 8108116, Ann Arbor, MI

Collett, T.S., 2002 Energy resource potential of natural gas hydrates. AAPG Bull. 86 (11): 1971-1992.

Collett, T., et al. (2008), Indian National Gas Hydrate Program Expedition 01 initial reports: Expedition 01 of the Indian National Gas Hydrate Program from Mumbai, India to Chennai, India; Sites NGHP-01-01 through NGHP-01-21, April 2006 –August 2006, Dir. Gen. of Hydrocarbons, Minist. of Pet. and Nat. Gas, Noida, India.

Dallimore, S. R., Collett, T. S., and Uchida, T., (1999), Overview of science program, JAPEX/JNOC/GSC Mallik 2L-38 gas hydrate research well, in Scientific Results From JAPEX/JNOC/GSC Mallik 2L-38 Gas Hydrate Research Well, Mackenzie

Delta Northwest Territories, Canada, edited by S. R. Dallimore et al., Bull. Geol. Surv. Can., 544, 11–17.

Frank, H.S., Evans, M.W.,(1945) J. Chem. Phys., 13, 507

Guerin, G., D. Goldberg, and A. Meltser (1999), Characterization of in situ elastic properties of gas hydrate-bearing sediments on the Blake Ridge, J. Geophys. Res., 104, 17,781 – 17,795

Hanse, J.-P., McDonald, I.R., (2006). Theory of Simple Liquids, Elsevier, Oxford, UK

Hammerschmidt, E.G., 1934. Formation of gas hydrates in natural gas transmission lines. Ind. Eng. Chem. 26, 851–855.

Helgerud, M. B., J. Dvorkin, A. Nur, A. Sakai, and T. Collett (1999), Elastic-wave velocity in marine sediments with gas hydrates: Effective medium modeling, Geophys. Res. Lett., 26, 2021–2024.

Hill, R. (1963), Elastic Properties of Reinforced Solids: Some theoretical Principles. J. Mech. Phys. Solids, 1963, Vol. 11 pp 357-3752

Kleinberg, R. L., and J. Dai (2005), Estimation of the mechanical properties of natural gas hydrate deposits from petrophysical measurements, paper OTC 17205 presented at the Offshore Technology Conference, Am. Assoc. of Pet. Geol., Houston, Tex.

Kneafsey, T. J., L. Tomutsa, G. J. Moridis, Y. Seol, B. M. Freifeld, C. E. Taylor, and A. Gupta (2007), Methane hydrate formation and dissociation in a partially saturated core-scale sand sample, J. Petrol. Sci. Eng., 56, 108 – 126.

Lee, M. W., and W. F. Waite (2008), Estimating pore-space gas hydrate saturations from well log acoustic data, Geochem. Geophys. Geosyst. 9

Lunne, T., Berre, T., Andersen, K.H., Strandvik, S., Sjursen, M. (2006). Effects of sample disturbance and consolidation procedures on measured shear strength of soft marine Norwegian clays. Canadian Geotechnical Jouranl 43: 726-750

Makogon, Y.F., (1965). A gas hydrate formation in the gas saturated layers under low temperature. Gas Indus. 5, 14–15.

Makogon, Y.F., (1966). Peculiarities of Gas-Field Development in Permafrost. Nedra, Moscow.

Makogan, Y.F., Hydrates of Natural Gas, Moscow, Nedra, Izadatelstro, PennWell Books, Tulsa, Oklahoma, p. 237 in Russian (1981 in English) (1974).

Makogon, Y.F., (1997). Hydrates of Hydrocarbons. Penn Well, Tulsa, USA, 10-16

Makogon Y.F., Holditch S.A., Lee S.Y., (2001). Gas Solubility and Hydrate Deposits Formation, IGRC-November, 2001 Amsterdam.

Makogon Y.F., (2010). Natural gas hydrates-A promising source of energy.Journal of Natural Gas Science and engineering 2, 49-59

Moridis, G.J., Collett, T.S., Pooladi-Darvish, M., Hancock, S.H., Santamarina, C., Boswell, R., Kneafsey, T.J., Rutqvist, J., Kowalsky, M.B., Reagan, M.T., Sloan, E.D., Sum, A., Koh, C., (2010). Challenges, uncertainties, and issues facing gas production from gas-hydrate deposits. SPE Reservoir Eval. Eng. 14 (1), 76–112.

Murray, D. R., R. L. Kleinberg, B. K. Sinha, M. Fukuhara, O. Osawa, T. Endo, and T. Namikawa (2006), Saturation, acoustic properties, growth habit, and state of stress of a gas hydrate reservoir from well logs, Petrophysics, 47, 129–137.

Priestley, J., (1778–1780). Versuche und Beobachtungen Uber Verrshiedene Gattungen der Luft, Th. 1-3, 3:359–362. Wien-Leipzig.

Ripmeester, J., Ratclife, C., Klug, Tse, J., (1994). II-nt. GHC, N-Y.

Rodger, M., (2000). in Proc. Gas Hydrates: Challenges for the Future, (Holder, G.D., Bishnoi, P.R.,eds), Ann. N.Y. Acad. Sci., 912, 474

Rutqvist, J., Grover, T., Moridis, G.J. (2008). Coupled Hydrological, Thermal and Geomechanical Analysis of Wellbore Stability in Hydrate-Bearing Sediment, OTC 19672, Proc. 2008 Offshore Technology Conference, Houston, 4-8 May 2008

Salzmann, C.G., Radelli, P.G., Mayer, E., and Finnely, J.L. (2009), Ice XV: a new thermodynamically stable phase of ice. Phys Rev Letter 103(10):105701

Seol Y., Myshakin E., (2011). Experimental and numerical obervations of hydrate reformation during depressurization in a core-scale reactor, Energy & Fuels. volume 25. 1099-1110

Servio, P., and P. Englezos (2002), Measurement of dissolved methane in water in equilibrium with its hydrate, J. Chem. Eng. Data, 47, 87–90,

Tréhu, A.M, Bohrmann, G., Rack, F.R., Torres, M.E., et al., (2003). Shipboard Scientific Party, Explanatory notes Proc. ODP, Init. Repts., 204: College Station, TX (Ocean Drilling Program), 1–102. doi:10.2973/odp.proc.ir.204.102.2003

Sloan, E. D., and C. A. Koh (2008), Clathrate Hydrates of Natural Gases, 3rd ed., 721 pp., CRC Press, Boca Raton, Fla.

Stillinger, F.H., and Weber, T.A. (1980), Lindemann Melting Criterion and the Gaussian core model, Physical Review B., volume 22, 3790-3794

Von Stackelberg, M., 1949–1954. Solid gas hydrates. Zeitschrift Elektrochem 58, 104.

Waite, W. F., W. J. Winters, and D. H. Mason (2004), Methane hydrate formation in partially water-saturated Ottawa sand, Am. Mineral., 89, 1202–1207.

Winters, W.J., Waite, W.F., Mason, D. H., and Kumar, P., (2008), Physical properties of repressurized samples recovered during the 2006 national gas hydrate program expedition offshore India, paper 5531 presented at the 6th International Conference on Gas Hydrates, Chevron, Vancouver, B. C., Canada, 6–10 July.

Yuan, T., G. D. Spence, R. D. Hyndman, T. A. Minshull, and S. C. Singh (1999), Seismic velocity studies of a gas hydrate bottomsimulating reflector on the northern Cascadia continental margin: Amplitude modeling and full waveform inversion, J. Geophys. Res., 104, 1179–1191, doi:10.1029/1998JB900020.

Yun, T. S., F. M. Francisca, J. C. Santamarina, and C. Ruppel (2005), Compressional and shear wave velocities in uncemented sediment containing gas hydrate, Geophys. Res. Lett., 32, L10609, doi:10.1029/2005GL022607.

Yun, T. S., J. C. Santamarina, and C. Ruppel (2007), Mechanical properties of sand, silt, and clay containing tetrahydrofuran hydrate, J. Geophys. Res., 112, B04106, doi:10.1029/ 2006JB004484

APPENDIX A

CHAPTER III MATERIALS

Appendix A consists of data and charts for Chapter 3

Appendix A.1 Labview Interface

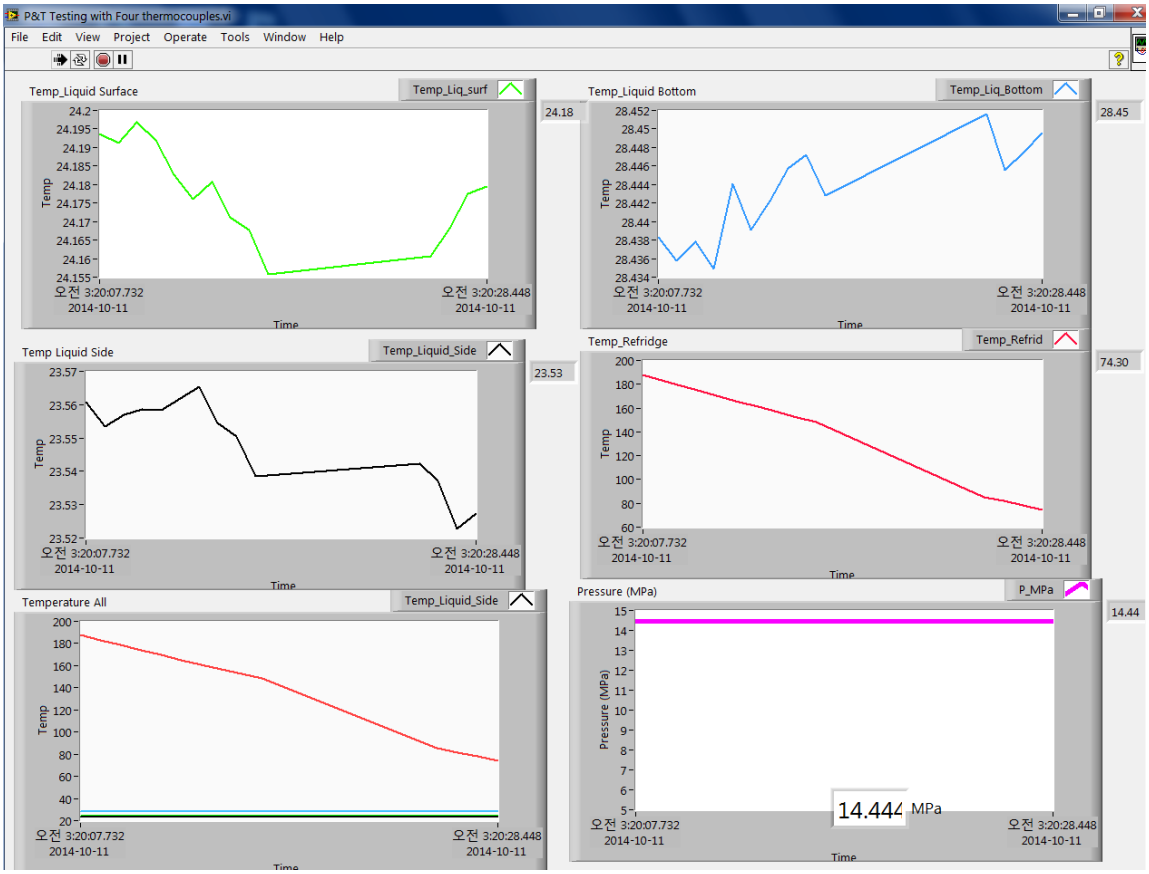

Figure A.1 Labview data display

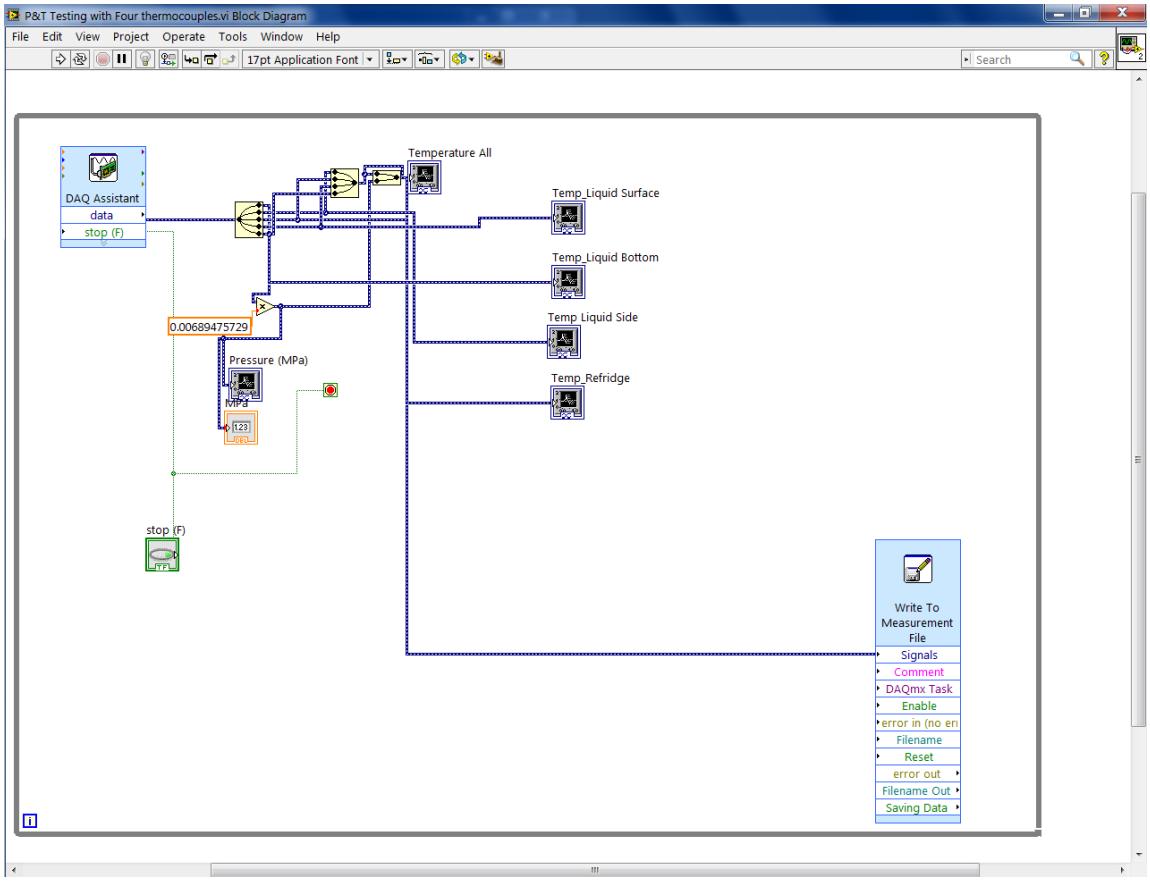

Figure A.2 Labview Block Diagram

Appendix A.2 ICE Experiment Result-Ice Formation

Experiment Description	COPPER TUBE		COPPER CYLINDER		
Experiment Date	08/21/2013	08/22/2013	09/06/2013	09/23/2013	09/24/2013
Formation Temperature (C)	-5	-6	-4	-6	-6
Initial Pressure (MPa)	0	0	0	14.26	14.32

Experiment Description	POROUD MEDIA WITH SAND, COPPER CYLINDER ON TOP						
Experiment Date	09/27/2013	09/28/2013	09/29/2013	09/30/2013	10/01/2013	01/01/2013	10/02/2013
Formation Temperature (C)	-3	-4	-0.5	0	-4	-4	-3
Initial Pressure (MPa)	3.9	3.8	0.048	0.048	14.24	13.71	3.94

Table A.1: Summary of ice experimental results after the installation of DAQ system.

Appendix A.3 Summarized Results of Hydrate Experiments

LOCATION	Hydrate Formation in the Beaker with Copper Cylinder on the Top of the Chamber							
Experiment	**1**	**2**	**3**	**4**	**5**	**6**	**7**	**8**
Date	10/18/2013	10/28/2013	10/30/2013	11/01/2013	11/05/2013	11/08/2013	11/09/2013	11/11/2013
Time Start	10:14	14:37	16:07	13:13	15:15	17:11	18:20	22:05
Time Formed	16:44	15:44	18:00	15:21	16:46	21:47	22:37	19:43
Time Duration	6:30	1:07	1:53	2:08	1:31	4:36	2:17	3:39
P at Start (MPa)	10.95	11.42	11.38	11.72	12.4	8.6	8.41	12.88
P at Formation (Mpa)	10.26	11.22	11.16	11.036	11.1	7.15	7.19	10.93
T initial (Celsius)	12.6	16.3	15.5	30	31	40	36	30
T formation (Celsius)	1	12.8	11.6	9.9	9.7	-3.2	-0.26	-3.5
T subcooling (Celsius)	13	0.3	1	4	4	13	13	16
Nucleation Sites (approx)	**20**	NO DATA	NO DATA	NO DATA	NO DATA	NO DATA	NO DATA	NO DATA
Nucleation Rate (mm/sec)	**2.09**	NO DATA	NO DATA	NO DATA	NO DATA	NO DATA	NO DATA	**1.891**

Table A.2: Summarized results of the hydrate experiment with copper cylinder on the top window

LOCATION	Hydrate Formation without the Beaker with Copper Cylinder on the Back of the Chamber			
Experiment	**9**	**10**	**11**	**12**
Date	11/29/2013	11/30/2013	12/01/2013	12/04/2013
Time Start	16:42	12:28	10:15	
Time Formed	18:46	13:02	10:54	
Time Duration	6:46	0:34	0:41	1:19
P at Start (MPa)	10.92	10.844	10.77	12.06
P at Formation (Mpa)	10.02	10.68	10.66	10.115
T initial (Celsius)	12.05	20.3	21	28.63
T formation (Celsius)	-0.57	11.1	11.31	3.706
T subcooling (Celsius)	13.5	2.4	2.2	10
Nucleation Sites (approx)	**50**	NO DATA	**20**	**40**
Nucleation Rate (mm/sec)	**1.194**	NO DATA	**0.09**	**0.918**
Temperature Hold	16 Hours	4 Hours		24 Hours

Table A.3: Summarized results of the hydrate experiment with copper cylinder on the back window

Appendix A.3 Hydrate Formation in the Beaker with Copper Cylinder on the Top of the Chamber

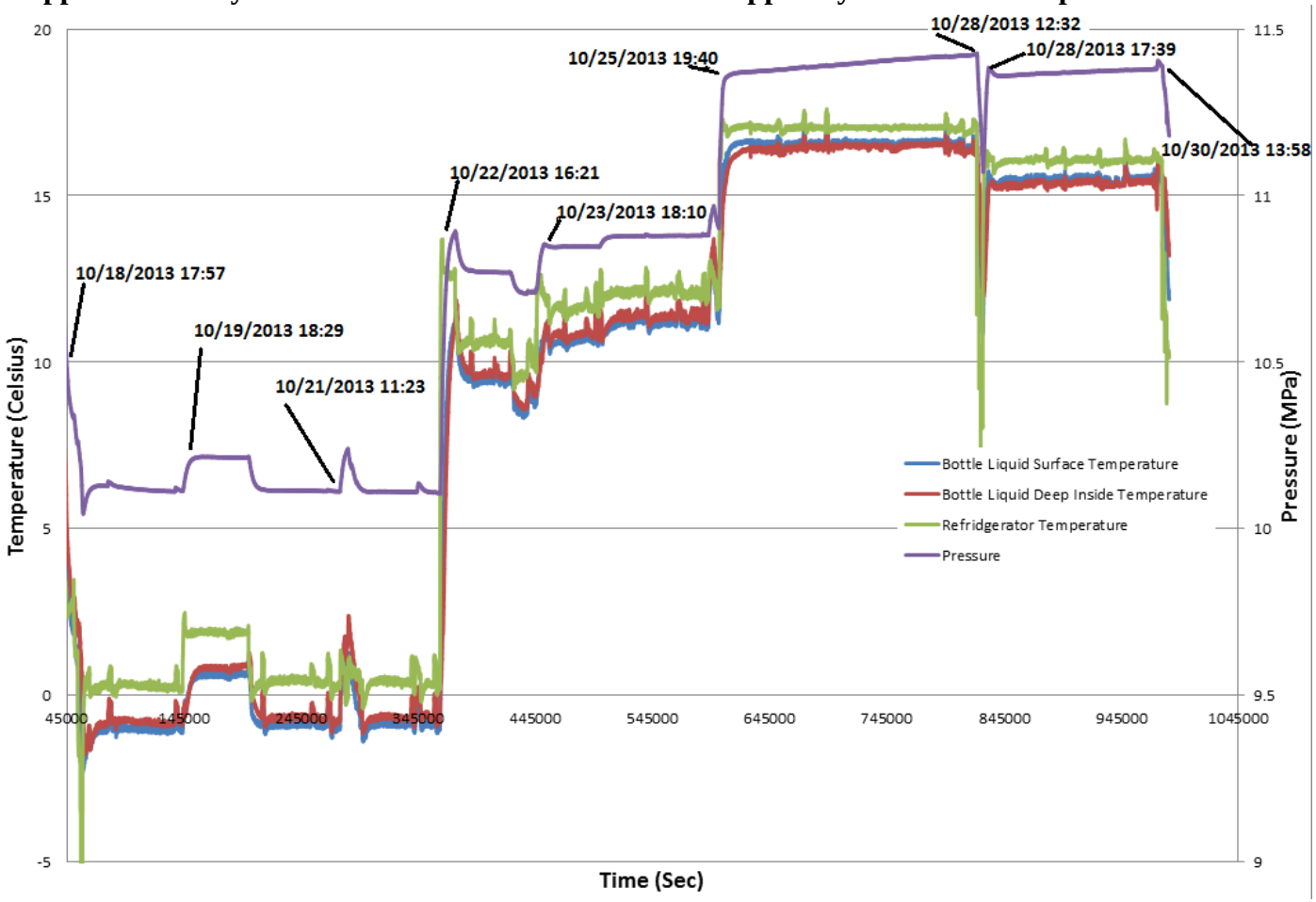

Figure A.3: Hydrate formation with beaker PART 1

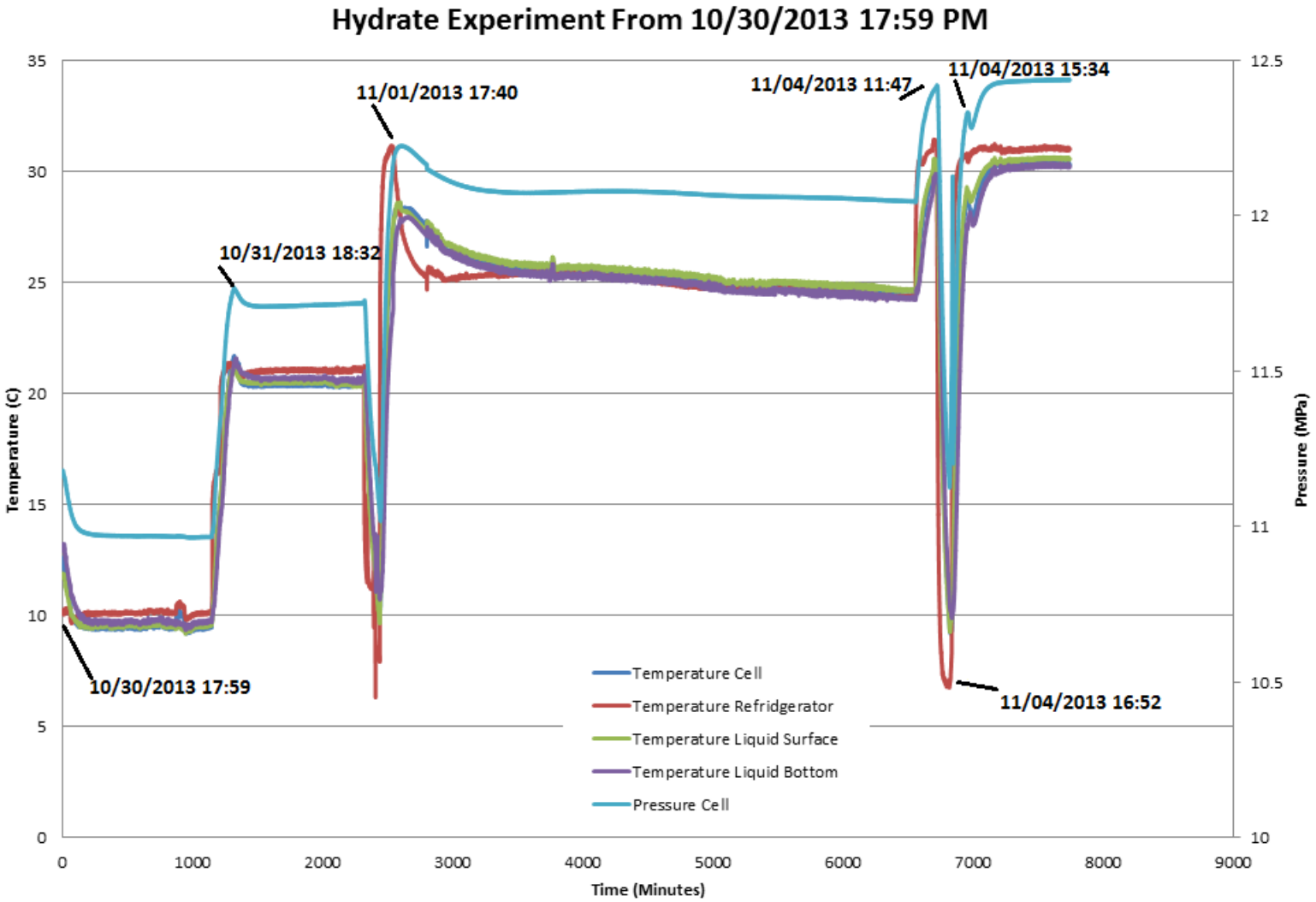

Figure A.4: Hydrate formation with beaker PART 2

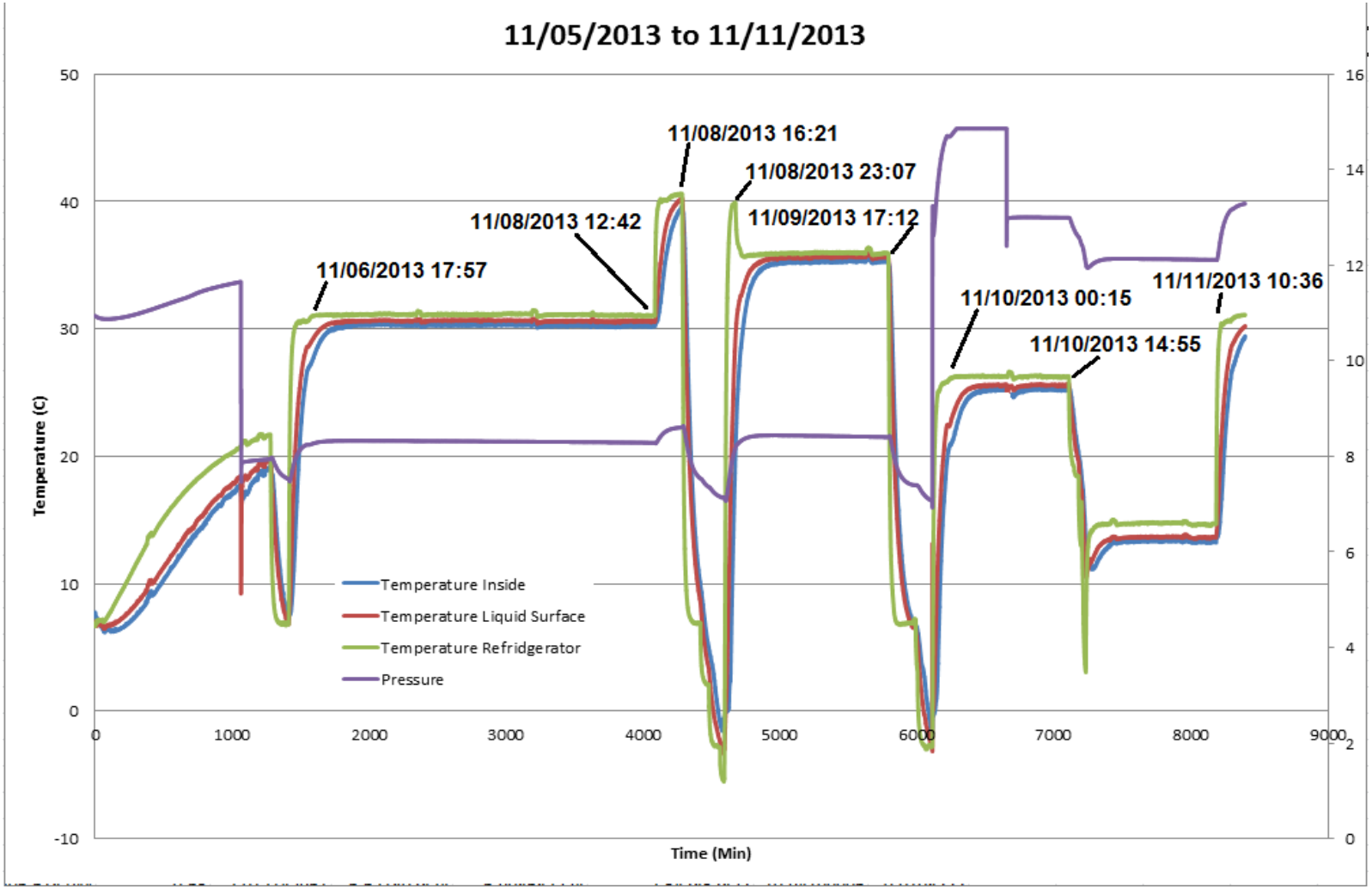

Figure A.5: Hydrate formation with beaker PART 3

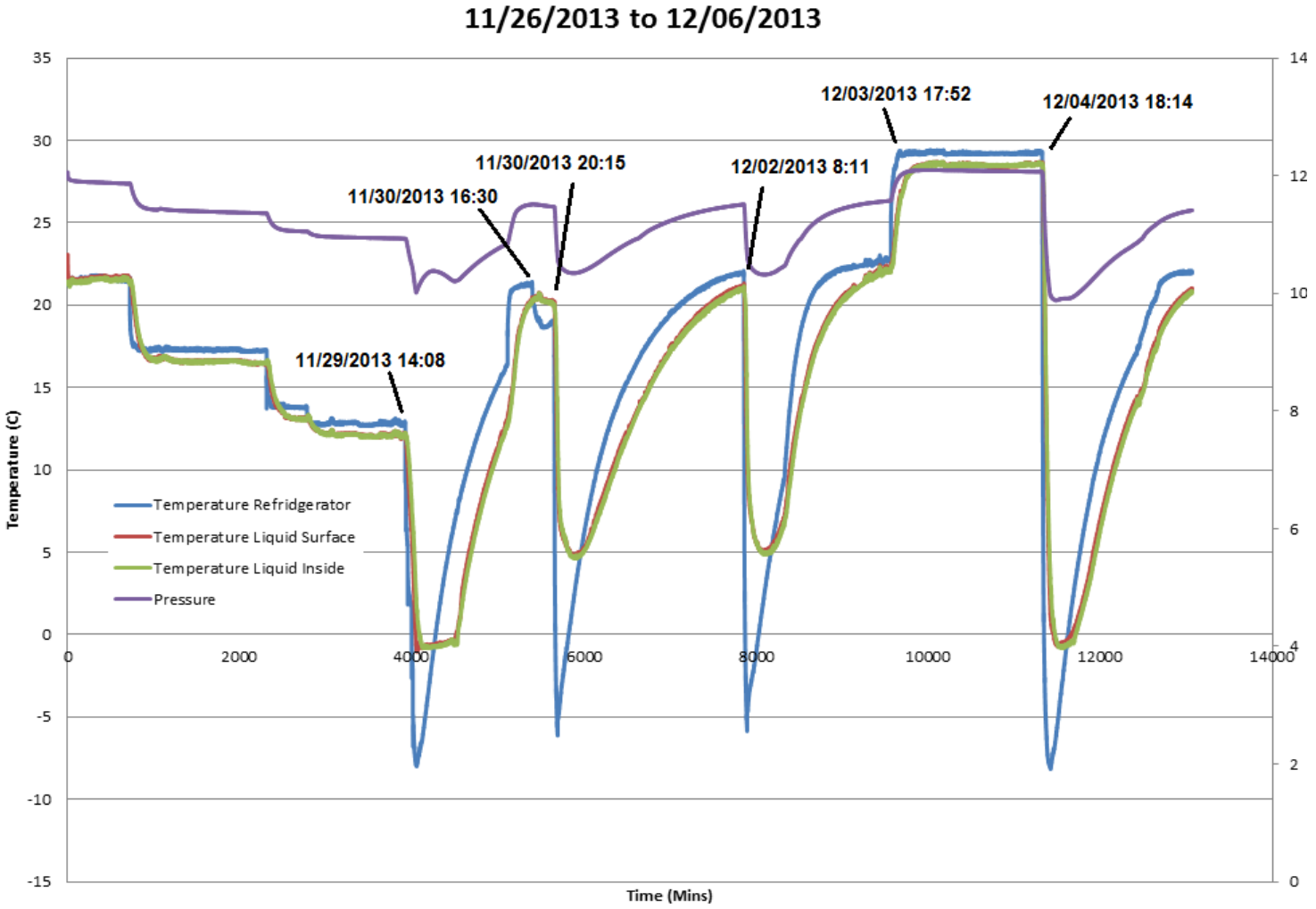

Figure A.6: Hydrate Formation without the beaker

A.4 Memory Effect Graph from Chapter 3 Data

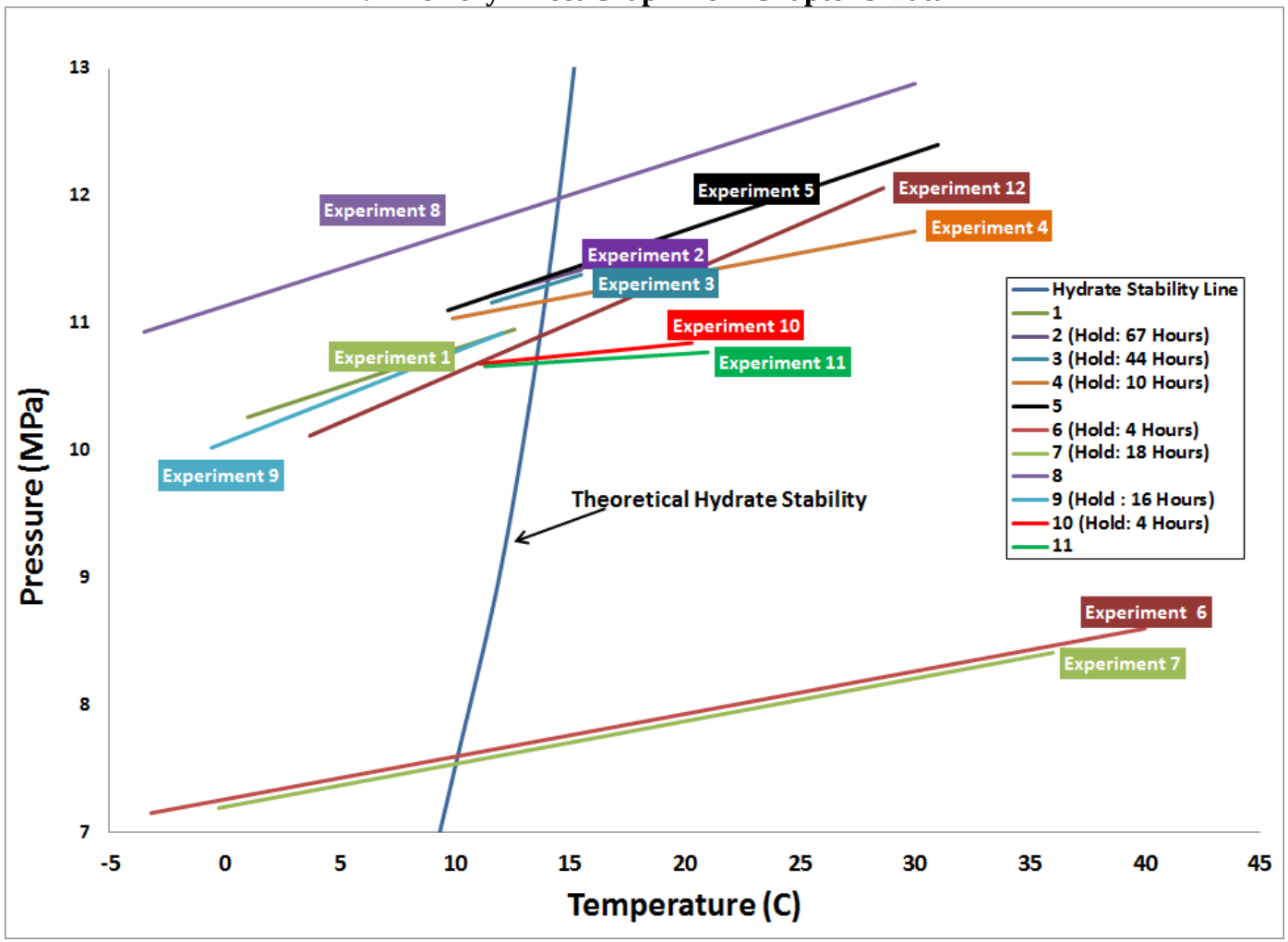

Figure A.7: Comparing memory effect in water-gas system. Each plot represents temperature change from initial condition to hydrate formation condition (from the right of the hydrate stability line to the left).

A.5 Analysis of Pressurized Ice Propagation

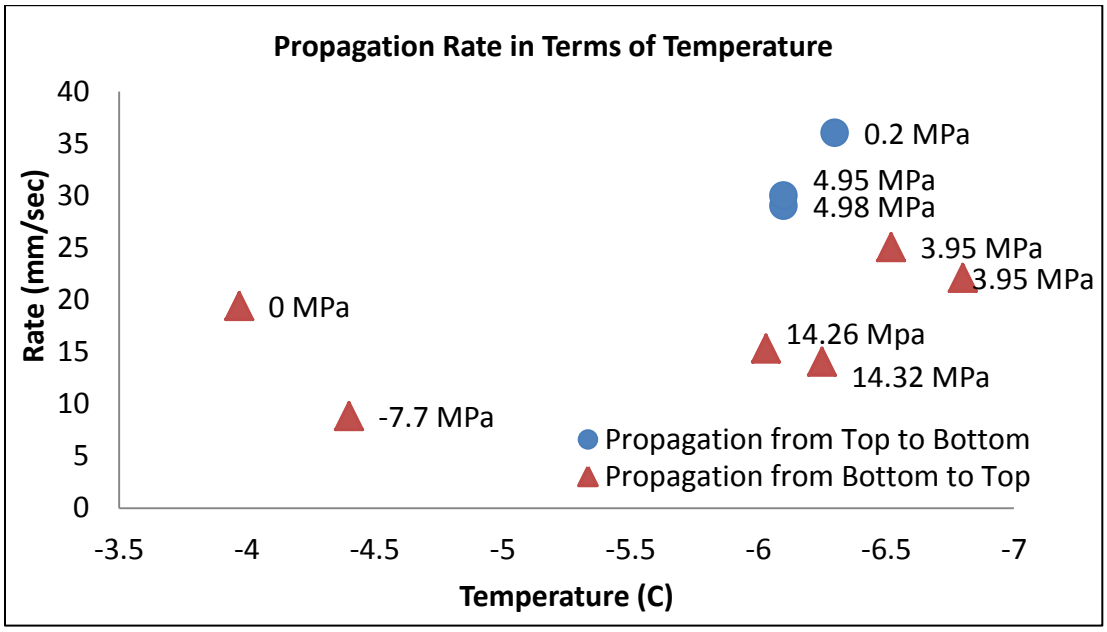

Figure A.8 Propagation rate in terms of temperature

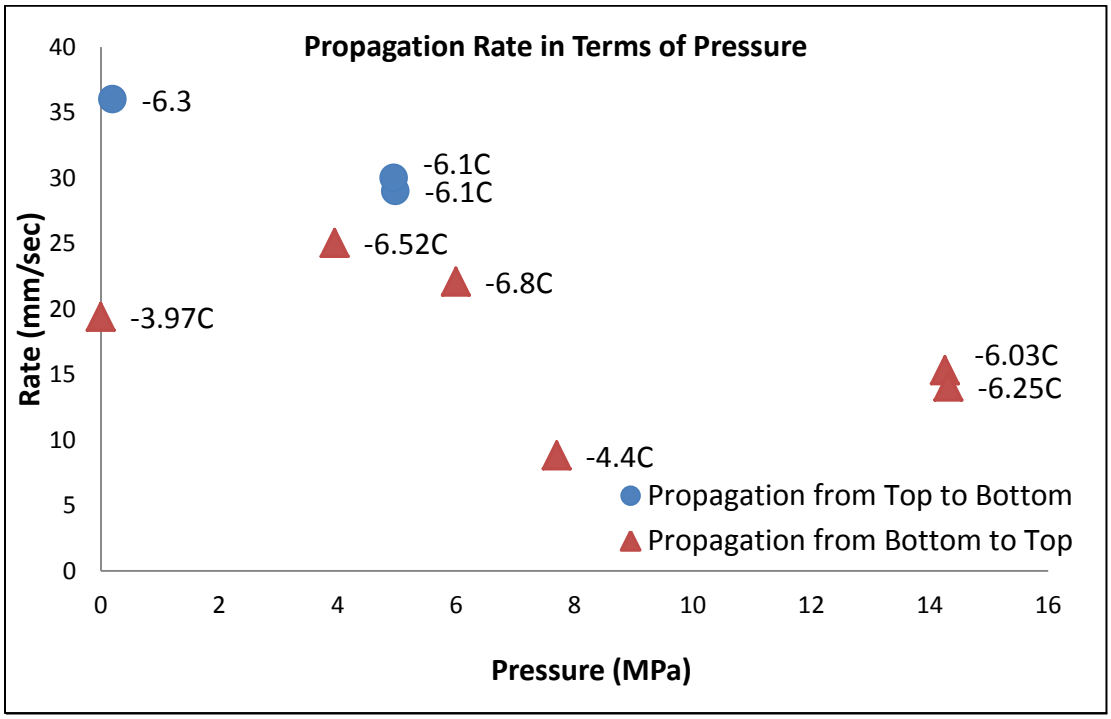

Figure A.9 Propagation rate in terms of pressure

Sample Ice formation graph from preliminary experiments. Only one graph is shown as an example.

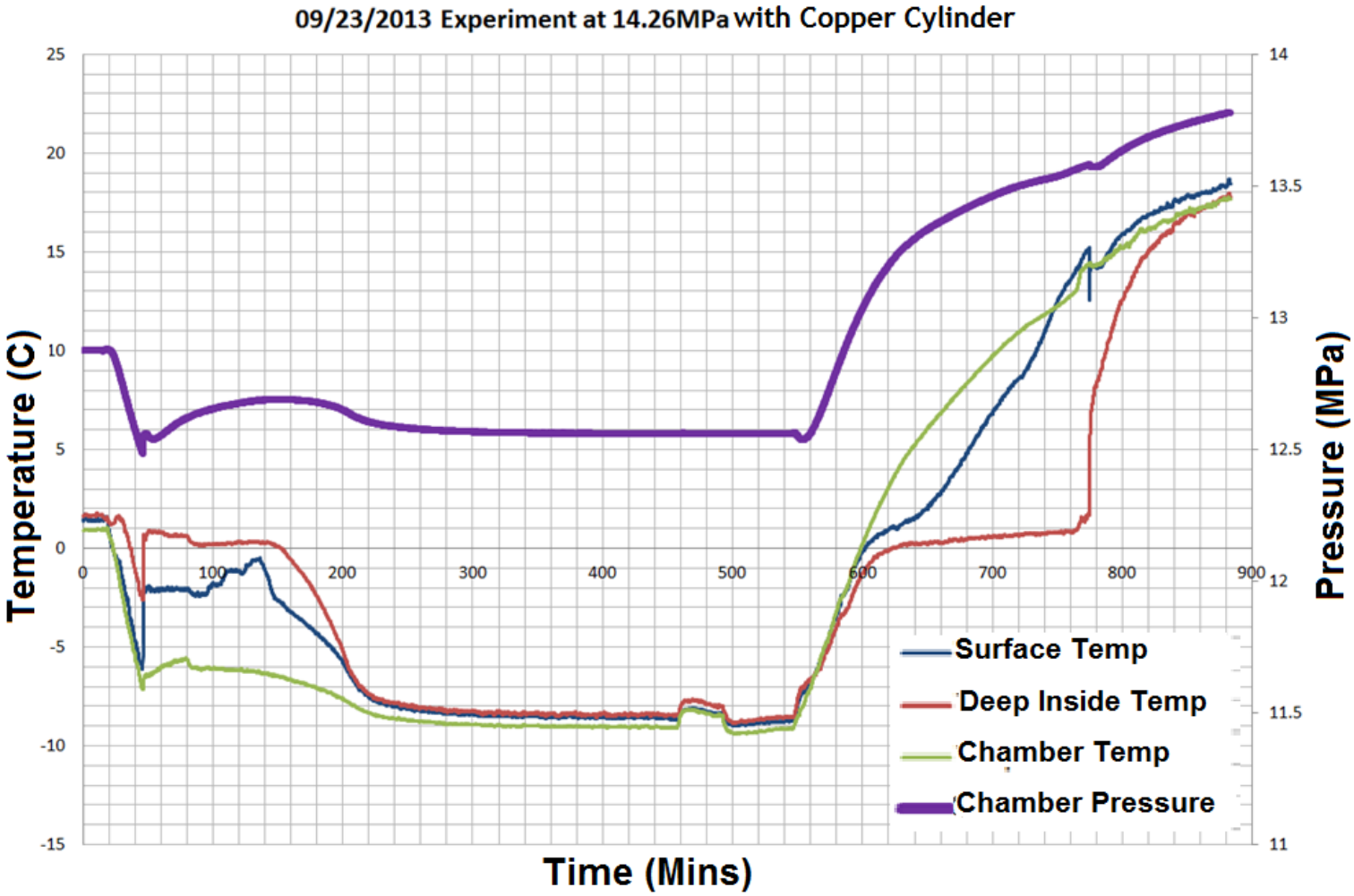

Figure A.10 Sample ice formation graph

APPENDIX B

CHAPTER VI MATERIALS

Appendix B consists of data for Chapter 4

Temp (Kelvin)	1(Pico Seconds)	3	7	10	20	40	100	140	200	250
293 (K)	0.0027	0.0059	0.0071	0.0043	-0.0089	-0.0028	0.0027	0.0036	0.0039	0.0038
313 (K)	0.0044	0.0090	0.0079	0.0065	0.0043	0.0119	0.0149	0.0166	0.0181	0.0183
343 (K)	0.0218	0.0300	0.0266	0.0250	0.0246	0.0266	0.0307	0.0311	0.0334	0.0357
373 (K)	0.0199	0.0308	0.0272	0.0256	0.0291	0.0359	0.0378	0.0411	0.0455	0.0480

200	250	300	350	400	500	1000	2000	4000	6000	8000	9000
0.0039	0.0038	0.0047	0.0054	0.0075	0.0084	0.0055	0.0140	0.0190	0.0222	0.0284	0.0323
0.0181	0.0183	0.0187	0.0186	0.0193	0.0203	0.0431	0.0493	0.0544	0.0522	0.0529	0.0532
0.0334	0.0357	0.0374	0.0381	0.0396	0.0416	0.0811	0.1039	0.1398	0.1558	0.1644	0.1659
0.0455	0.0480	0.0482	0.0529	0.0565	0.0674	0.0654	0.0956	0.1062	0.1087	0.1314	0.1763

10000	12000	14000	16000	18000	20000	25000	30000	35000	40000	45000	50000
0.0472	0.0667	0.0797	0.0872	0.0965	0.1043	0.1158	0.1239	0.1325	0.1389	0.1438	0.1479
0.0532	0.0636	0.0929	0.1183	0.1307	0.1420	0.1637	0.1968	0.2272	0.2508	0.2687	0.2833
0.1729	0.1857	0.1935	0.1983	0.2018	0.2039	0.2128	0.2192				
0.2022	0.2638	0.3205	0.3582	0.3840	0.4042						

60000	70000	80000	90000
0.1537	0.1577	0.1608	0.1635

Table B.1 Lindemann's Number data for various temperature points

APPENDIX C

CHAPTER V MATERIALS

Appendix C consists of data and charts for Chapter 5

Appendix C.1 Labview Interface

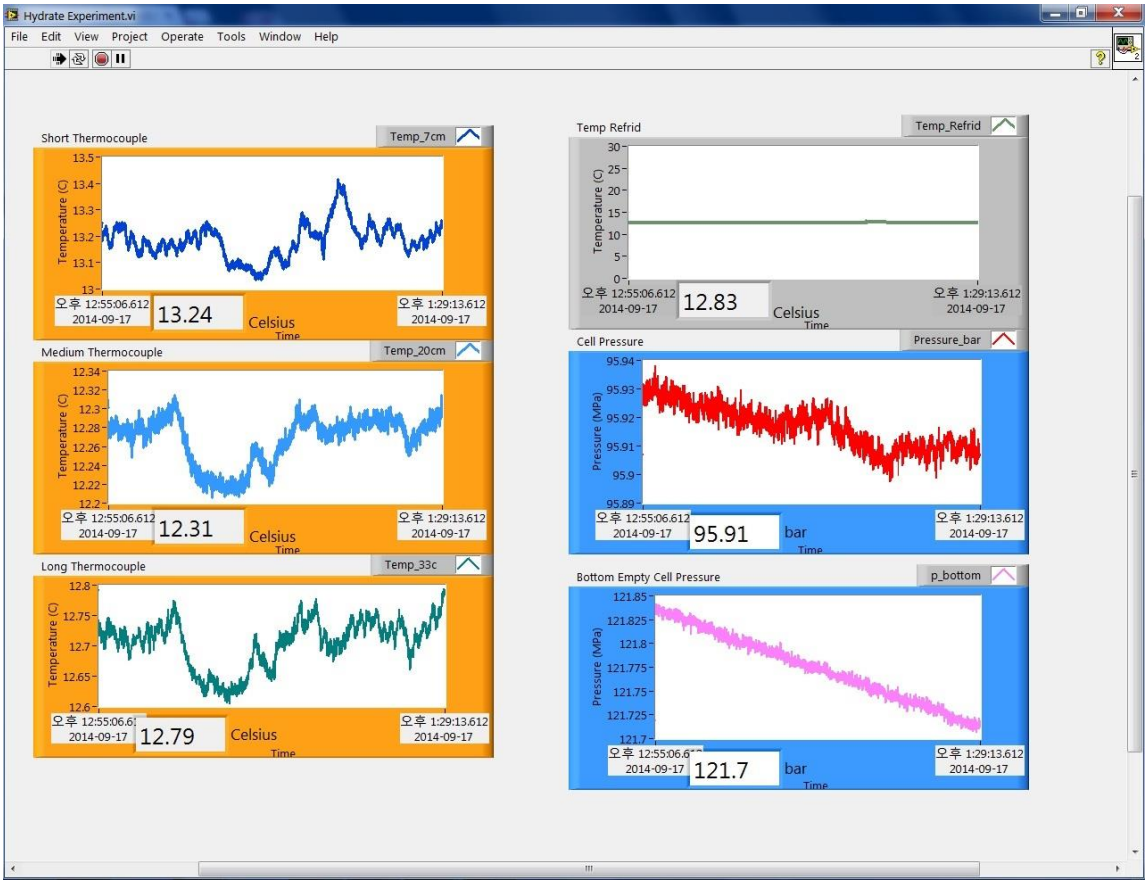

Figure C.1 Screenshot of Labview data collection interface

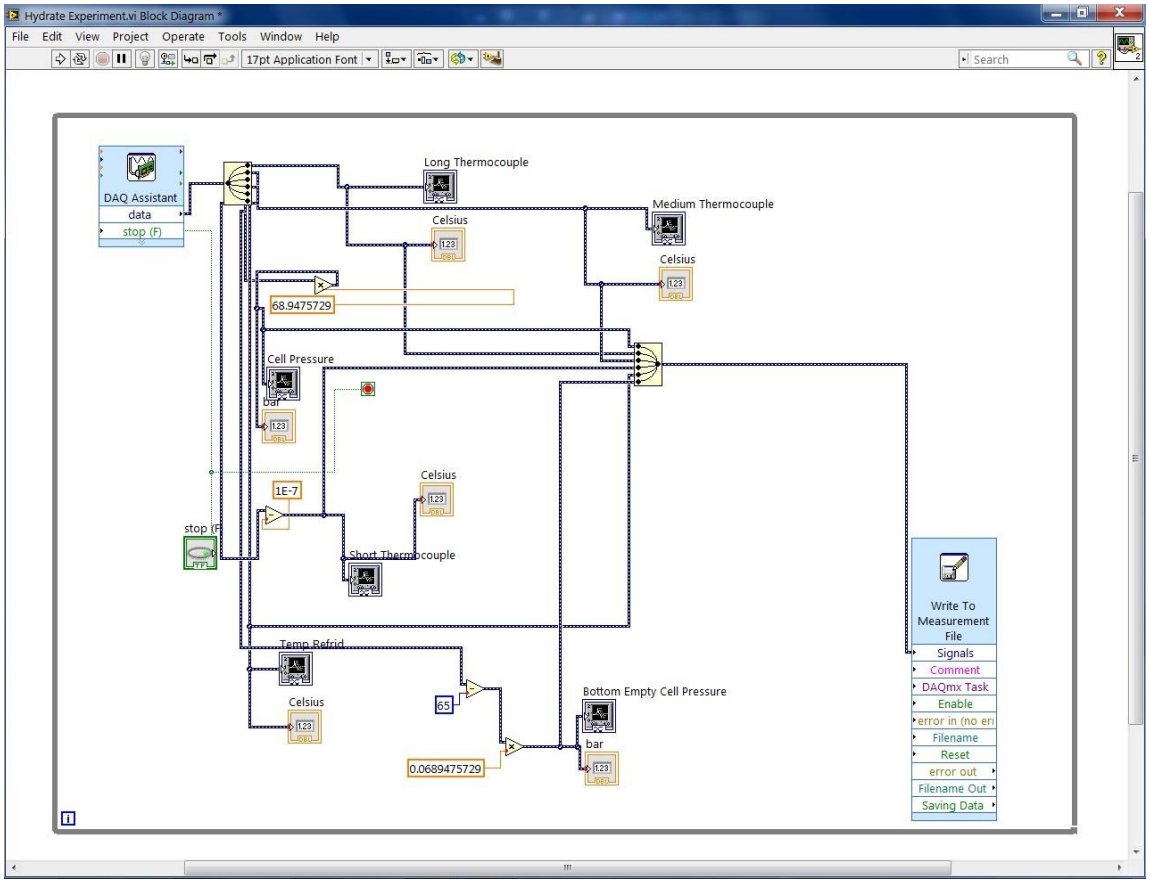

Figure C.2 Labview block diagram

Appendix C.2 Hydrate Experiment in pore-space experimental graphs

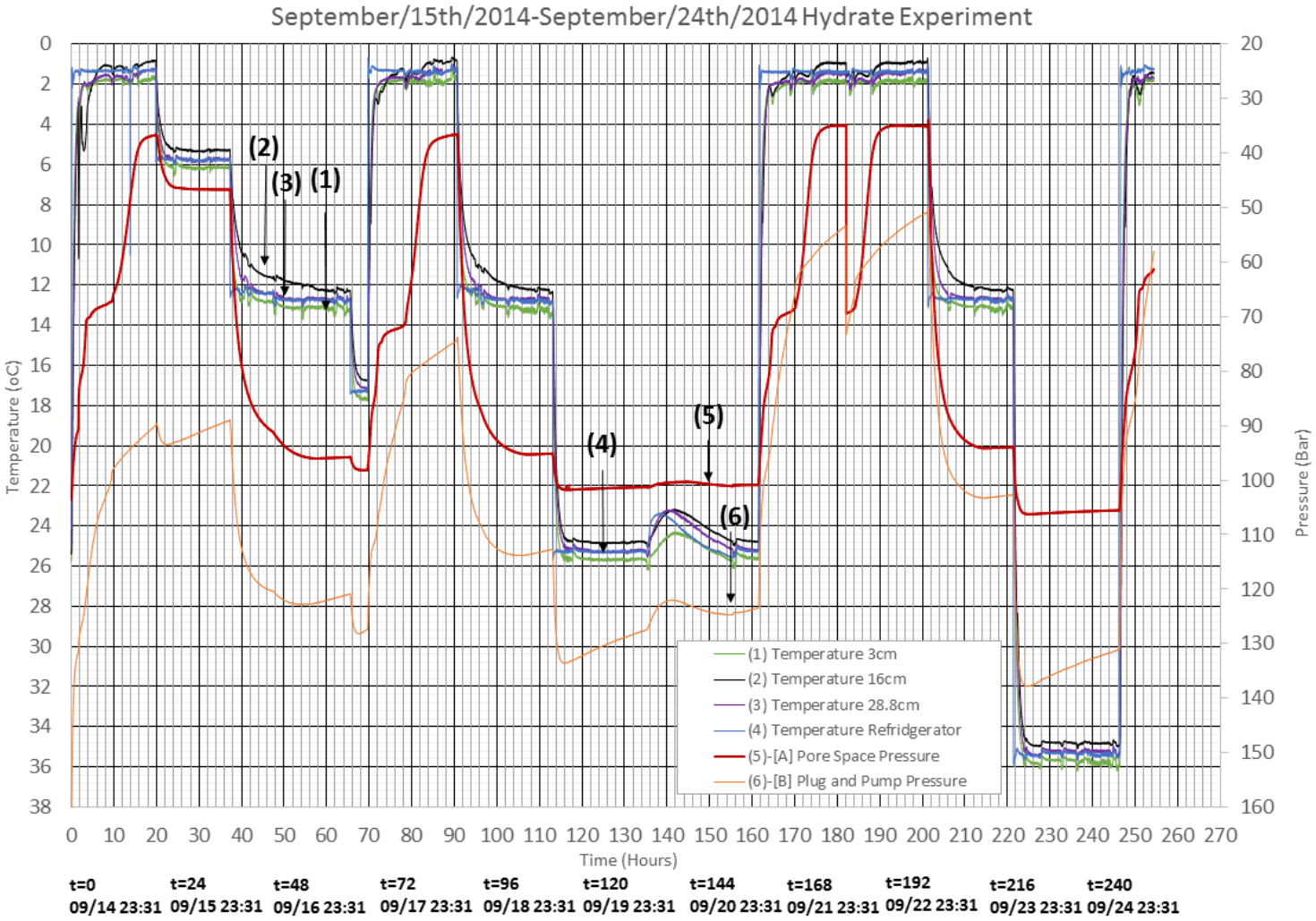

Figure C.3 : Hydrate experiment result in pore-space part 1

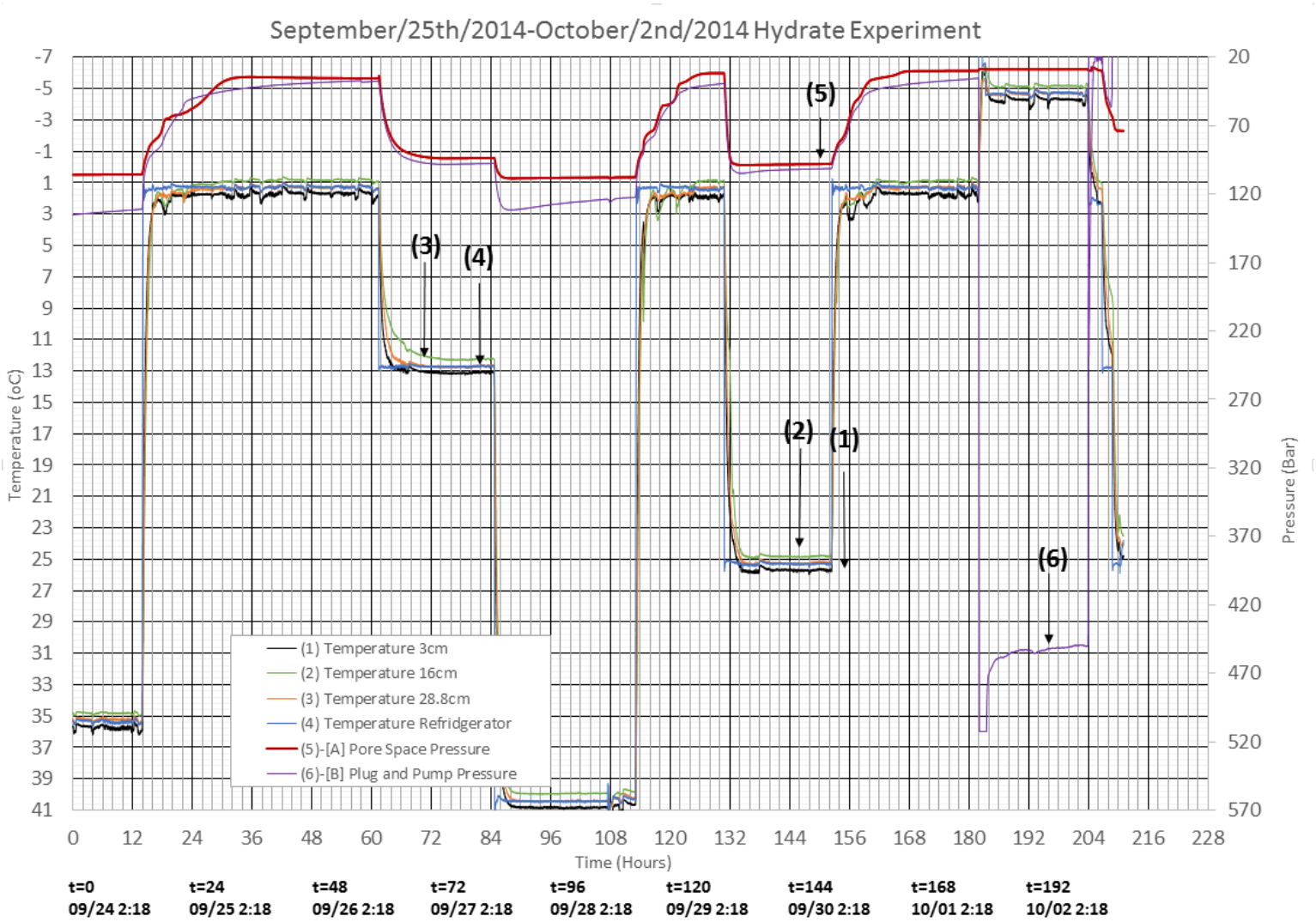

Figure C.4 : Hydrate experiment result in pore-space part 2

APPENDIX D

CALCULATIONS AND CONSIDERATIONS

D.1 Stress Analysis and Calculation for Stainless Steel Cylinder Used in Chapter 5

The volume of chamber is 1.368 liters, (or 1,368,303 mm^3). If the chamber is completely filled with water alone, when the temperature is brought down to freezing point, on average there will be 9% volume increase so with chamber in the lab, 1.368liters of water will freeze to occupy 1.491liters of ice. In comparison if the entire volume of the chamber is filled with dissolved methane and water to form 100% hydrate in the chamber, the volume increase will be 26%.

The density of pure frozen ice is about $0.9167\frac{g}{cm^3}$, where the pure water has density of $0.9998\frac{g}{cm^3}$ (both at 0 C). The density of methane hydrate is about $0.917\frac{g}{cm^3}$ as same condition

The chamber in lab 721 is made with stainless steel, the general stainless steel properties were used to calculate the stress that it can withstand in the assumption that the whole chamber is filled with water then the temperature is brought down to turn to complete ice as Dr. Makogon requested. The general properties are shown below, with dimensions of the chamber,

Ultimate Tensile Strength	505 MPa
Yield Tensile Strength	215 MPa
Poisson's Ratio	0.29
Shear Modulus	86 GPa

Table D.1: Mechanical properties of stainless steel

Figure D.1: Measurements of the stainless steel cylinder used in chapter 5

There are more than 10 types of ice that exists. Assuming that ice in the stainless steel chamber is NOT going to be pressured by nitrogen and that the water is frozen in chamber without any disturbance within the cell (other than the chamber wall) and is frozen by just the temperature decrease, it can be assumed that it will remain at ordinary ice I_h

The chamber in Lab 721 is in cylindrical shape, it will be prone to both axial and circumferential stresses. Thin wall assumption can be implied if the outer diameter of the cylinder, D and the thickness of the cylinder, t, has the relationship of $D/t>10$. However, from the chamber in Lab 721, the Outer diameter is 93.46mm and the thickness of the vessel is 11.842mm, $D/t<10$ hence simple thin walled assumption cannot be made. Thick walled cylinder assumption is needed to be used, in the thick walled assumptions, The axial stress is defined as,

$$\sigma_a = \frac{p_i r_i^2 - p_o r_o^2}{r_o^2 - r_i^2}$$

The radial stress is defined as,

$$\sigma_r = \left[\frac{p_i r_i^2 - p_o r_o^2}{r_o^2 - r_i^2}\right] - \left[\frac{r_i^2 r_o^2 (p_o - p_i)}{r^2 (r_o^2 - r_i^2)}\right]$$

In this case of chamber being filled 100% with water will give uniform stress within the chamber when water freezes, (where with non-uniform formation of ice or hydrate in packed sand will yield distributed stress, hence requiring more detailed analysis of applied stress)

The necessary variables for the stress calculations are,
p_i= Pressure from inside,
r_i=Inner radius of the chamber
r_o=Outer radius of the chamber
r=radius of interest (r_i will be used to determine maximum possible stress)
There will be no pressure exerted from outside of the chamber, hence p_o, pressure from outside, can be disregarded

With dimensions of the stainless chamber and the maximum pressure exerted by ice, the maximum stress applied to chamber will be,
σ_a= 268 MPa , Axial direction
σ_r = 749 MPa, Radial direction

This is over the mechanical properties of the stainless steel. Not only will this chamber elongate, there will be burst from radial direction (circumferentially) hence, completely filling the chamber with water then freeze to ice in stainless steel is not safe.

Likewise, the calculations have been done if the chamber is completely filled with hydrates initially, then dissociate to release gas.

If the cell in the lab 721 is 100% filled with methane hydrate at 26 bar (2.6 MPa) at the temperature of 0C, when the hydrate dissociates, the pressure increases up to 1600 bar (160 MPa)

With dimensions of the stainless chamber and the maximum pressure exerted by ice, the maximum stress applied to chamber will be,
σ_a=178 MPa , Axial direction
σ_r =515 MPa, Radial direction

If all of the methane hydrate dissociates in the 100% methane hydrate filled stainless steel cell. This would cause burst in circumferential direction. However, bit less pressure

when compared with worst case scenario of 100% water being freezing to ice in the stainless cell. (749 MPa compared to 515 MPa).

D.2 Density Considerations for Methane Hydrates for Experiments

One unit volume of methane hydrate at a pressure of 26bar (2.6MPa) at 0 C contains 164 volumes of methane gas. Which in hydrate form 80%, by volume, is occupied by water and 20% by gas. Which in means in $1m^3$ of methane hydrate, 20% of its volume, $0.2m^3$, will contain $164m^3$ of gas.

In methane hydrate, on average, there exists 1 mole of methane for every 5.75 moles of water (MW of CH4 is 16.04g where MW of H20 is 18.04g).
The dissociation Pressure of methane hydrate at 273K or -0.15C is 2.56MPa.
The density values of methane hydrate at different pressure is listed below

1MPa	0.895 g/cm^3
10MPa	0.917 g/cm^3
100MPa	0.95 g/cm^3
1000MPa	1.053 g/cm^3

Table D.2: Density of methane hydrates at different pressures.